Biological Psychiatry: Celebrating 50 Years

Archival Report

Chronic Stress Causes Projection-Specific Adaptation of Amygdala Neurons via Small-Conductance Calcium-Activated Potassium Channel Downregulation

Wen-Hua Zhang, Wei-Zhu Liu, Ye He, Wen-Jie You, Jun-Yu Zhang, Hong Xu, Xiao-Li Tian, Bao-Ming Li, Lin Mei, Andrew Holmes, and Bing-Xing Pan

ABSTRACT

BACKGROUND: The role of the amygdala in mediating stress coping has been long appreciated. However, basolateral amygdala (BLA) projection neurons (PNs) are organized into discrete output circuits, and it remains unclear whether stress differentially impacts these circuits.

METHODS: Mice were exposed to acute restraint stress or chronic restraint stress (CRS), and c-fos expression was measured as a proxy for neuronal activation in Retrobead retrogradely labeled dorsomedial prefrontal cortex–targeting PNs (BLA→dmPFC) and non-dmPFC-targeting PNs (BLA↛dmPFC). Next, the effects of CRS on neuronal firing and membrane potassium channel current were examined via ex vivo electrophysiology in these neuronal populations and correlated with anxiety-like behavior, as measured in the elevated plus maze and novel open field tests. Lastly, the ability of virus-mediated overexpression of subtype 2 of small-conductance, calcium-activated potassium (SK2) channel in BLA↛dmPFC PNs to negate the anxiety-related effects of CRS was assessed.

RESULTS: BLA→dmPFC PNs were transiently activated after CRS, whereas BLA↛dmPFC showed sustained c-fos expression and augmented firing to external input. CRS led to a loss of SK2 channel–mediated currents in BLA↛dmPFC PNs, which correlated with heightened anxiety-like behavior. Virus-mediated maintenance of SK2 channel currents in BLA↛dmPFC PNs prevented CRS-induced anxiety-like behavior. Finally, CRS produced persistent activation of BLA PNs targeting the ventral hippocampus, and virally overexpressing SK2 channels in this projection population were sufficient to prevent CRS-induced anxiety-like behavior.

CONCLUSIONS: The current data reveal that chronic stress produces projection-specific functional adaptations in BLA PNs. These findings offer new insight into the neural circuits that contribute to stress-induced psychopathology.

Keywords: Amygdala, Anxiety, Circuit, Potassium channel, Prefrontal cortex, Stress

https://doi.org/10.1016/j.biopsych.2018.12.010

To effectively cope with psychological stress, the brain undergoes adaptations that promote function in regions subserving salience processing at a cost to areas responsible for cognition and executive control (1,2). These effects are reflected in the rapid engagement of brain regions involved in salience coding, such as the amygdala, striatum, midbrain, and brainstem, after stress exposure (3,4) and contrast with the functional downregulation that can occur in certain prefrontal cortical areas responsible for cognitive and executive control (5–7).

Importantly, the pattern and persistence of region-specific functional changes occurring in response to stress vary with stressor intensity and duration. Brief or mild stressors generally produce short-lasting effects that quickly normalize (8,9), whereas chronic and intense stress regimens produce lasting structural and functional remodeling in various brain regions, resulting in attendant emotional and behavioral deficits (10–12). These latter, more durable, effects of chronic stress are thought to contribute to the neuropathology of stress-related psychiatric diseases, ranging from major depression to anxiety disorders (13,14). Nonetheless, it remains unclear how stress-induced adaptations manifest at the level of specific brain circuits.

Technical advances that allow for cellular and circuit-specific manipulations have revealed that neuronal subpopulations in brain regions affected by stress, including the amygdala, are highly heterogeneous with regard to their output targets and function (15–19). Within the basolateral amygdala (BLA), projection neuron (PN) subpopulations send projections to the medial prefrontal cortex (mPFC), ventral hippocampus (vHPC), and nucleus accumbens (NAc) with minimal collateralization (16). Moreover, specific BLA output circuits have been found to differentially encode positive (e.g., BLA→NAc) or negative (e.g., BLA→vHPC) valence (20,21). Valence signaling

SEE COMMENTARY ON PAGE 784

 ISSN: 0006-3223

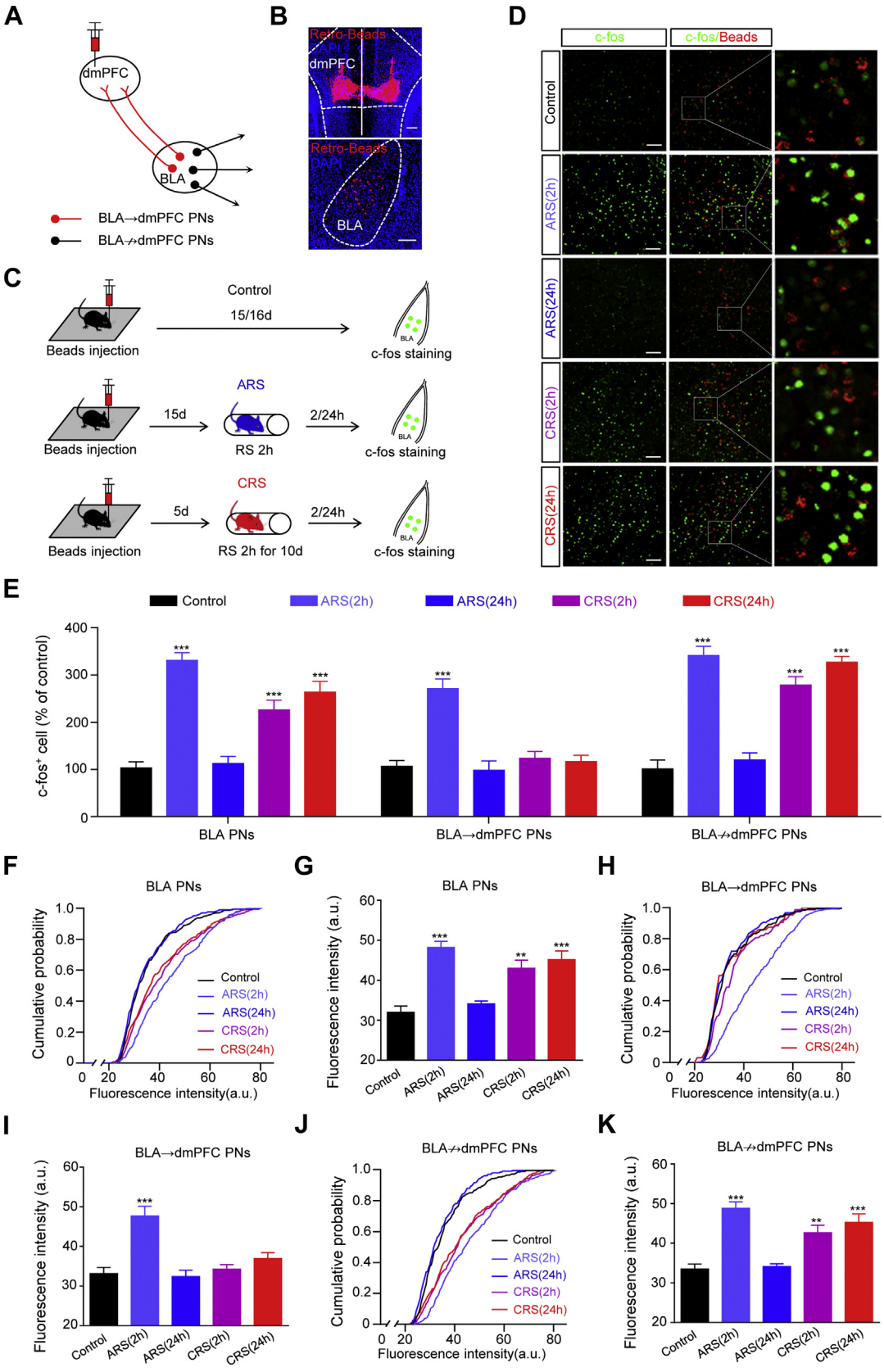
A
dmPFC
BLA
BLA→dmPFC PNs
BLA↛dmPFC PNs
B
Retro-Beads
DAPI
dmPFC
BLA
C
Control
15/16d
Beads injection
c-fos staining
ARS
15d
RS 2h
2/24h
CRS
5d
RS 2h for 10d
D
c-fos
c-fos/Beads
Control
ARS(2h)
ARS(24h)
CRS(2h)
CRS(24h)
E
c-fos+ cell (% of control)
BLA PNs
BLA→dmPFC PNs
BLA↛dmPFC PNs
F
BLA PNs
Cumulative probability
Fluorescence intensity(a.u.)
G
BLA PNs
Fluorescence intensity (a.u.)
H
BLA→dmPFC PNs
I
BLA→dmPFC PNs
J
BLA↛dmPFC PNs
K
BLA↛dmPFC PNs

to the mPFC may enable higher-order control and plasticity gating in subcortical structures, including, reciprocally, the BLA itself (22,23). However, while BLA neurons are known to be highly responsive to stress (4,24,25), the extent to which stress differentially impacts the function of discrete BLA PN subpopulations, including those targeting or evading the mPFC, is poorly understood.

To address this issue, we subdivided mouse BLA PNs based on whether or not their primary efferent target was the dorsomedial PFC (BLA→dmPFC vs. BLA↛dmPFC). We found that both populations are activated by acute restraint stress (ARS) but normalize within a day, whereas, in contrast, BLA↛dmPFC PNs remain persistently active after chronic restraint stress (CRS). We then showed that the lasting activation in BLA↛dmPFC PNs is associated with downregulation of subtype 2 of small-conductance, calcium-activated potassium (SK2) channel currents and that viral-mediated expression of SK2 channel in BLA↛dmPFC PNs, or specifically in the BLA→vHPC population, suffices to protect against the behavioral effects of chronic stress. Finally, we found that BLA PNs projecting to the vHPC, but not the NAc, exhibit SK channel downregulation after chronic stress in a manner correlating with increased anxiety-like behavior.

METHODS AND MATERIALS

Animals

All experimental procedures were approved by the Institutional Animal Care and Use Committee of Nanchang University. Subjects were male C57BL/6J mice (at least 5–6 weeks of age) housed in groups of three to five per cage with ad libitum access to food and water and maintained in a temperature- and humidity-controlled room with a light/dark cycle of 12 hours.

Restraint Stress, Stereotaxic Retrobeads Injection, and Anxiety-like Behavior

The procedures for restraint stress, injections of stereotaxic Retrobeads (Lumafluor Inc., Durham, NC), and anxiety-like behavior testing were performed as described previously (26) and are described in Supplemental Methods.

c-fos Immunohistochemical Staining

Coronal brain sections (30 μm) containing the whole amygdala were prepared, washed three times in phosphate-buffered saline (3 × 5 minutes), and blocked in permeable buffer (0.1% Triton X-100 in phosphate-buffered saline) containing 10% normal donkey serum for 2 hours at room temperature. Sections were incubated with the primary antibody against c-fos (1:500) overnight at 4°C, followed by three washes in phosphate-buffered saline Triton X-100 (Sigma-Aldrich, St. Louis, MO) and incubation with the fluorescent secondary antibody at room temperature for 2 hours. Sections were washed three times in phosphate-buffered saline Triton X-100 before being mounted onto the slides with Fluoromount Aqueous Mounting Medium (Sigma-Aldrich, St., Louis, MO). Confocal immunofluorescence images were taken by using a scanning laser microscope (Olympus FV1000; Olympus Corp., Tokyo, Japan). The c-fos fluorescence intensity in individual cells was calculated by using the same software with equal cutoff threshold being used to remove the background autofluorescence.

Ex Vivo Electrophysiology and Optogenetics

Ex vivo electrophysiologic recordings were performed as reported previously (10) and are described in Supplemental Methods.

Viral-Mediated SK2 Channel Rescue in Specific Subsets of BLA PNs After Stress

To express SK2 channel in BLA↛dmPFC PNs, a retrogradely traveling adeno-associated virus (AAV) vector, $AAV_{2/1}$-retro-Syn-EYFP-Cre, was bilaterally injected (0.3 μL per hemisphere) into the dmPFC, and Cre-Off $AAV_{2/8}$-CaMKIIα-DO-SK2-mCherry vector (or $AAV_{2/8}$-CaMKIIα-DO-mCherry control) was bilaterally injected (0.3 μL per hemisphere) into the BLA. To express SK2 channel in BLA→vHPC PNs, $AAV_{2/1}$-retro-Syn-EYFP-Cre vector was bilaterally injected into the vHPC, and Cre-On $AAV_{2/8}$-CaMKIIα-DIO-SK2-mCherry vector (or $AAV_{2/8}$-CaMKIIα-DIO-mCherry control) was bilaterally injected into the BLA. Mice were sacrificed 4 weeks later for either microscopy or ex vivo slice electrophysiology recording to confirm the expression and function of SK2 re-expression. The retroviruses and Cre-Off/Cre-On viruses were custom

Figure 1. Chronic stress produces lasting neuronal activation in dorsomedial prefrontal cortex (dmPFC) nonprojecting basolateral amygdala (BLA) projection neurons (PNs). **(A)** Schematic showing injection of red Retrobeads to dmPFC to label dmPFC-projecting BLA PNs (BLA→dmPFC PNs). BLA PNs not labeled by Retrobeads are regarded as putative non–dmPFC-projecting PNs (BLA↛dmPFC PNs). **(B)** Representative images showing the injection sites in the bilateral dmPFC (top panel) and the BLA→dmPFC PNs labeled with Retrobeads (bottom panel). 4′,6-Diamidino-2-phenylindole (DAPI) staining was performed to outline the brain regions of interest. Scale bar = 100 μm. **(C)** Schematic showing the experimental procedure for unstressed control mice and mice subject to acute restraint stress (ARS) or chronic restraint stress (CRS). **(D)** Representative images showing c-fos expression in BLA merged with (middle panel) or without (left panel) fluorescent beads. Expanded images indicated with a square are shown in the right panel. Scale bar = 100 μm. **(E)** c-fos$^+$ cells in BLA→dmPFC PNs and BLA↛dmPFC PNs (n = 5 mice per group). Two-way analysis of variance (ANOVA); main effect of stress treatment: $F_{4,60} = 94.97$, $p < .001$; main effect of neuron population: $F_{2,60} = 43.29$, $p < .001$; interaction: $F_{8,60} = 8.64$, $p < .001$; Bonferroni post hoc comparison vs. control, ***$p < .001$. **(F)** Cumulative probability of c-fos fluorescence intensity in BLA PNs. Kolmogorov-Smirnov test vs. control: ARS (2 hours), $p < .001$; ARS (24 hours), $p = .299$; CRS (2 hours), $p = .013$; CRS (24 hours), $p = .024$. **(G)** Average c-fos fluorescence intensity in BLA PNs. One-way ANOVA; $F_{4,20} = 17.88$, $p < .001$; Bonferroni post hoc comparison vs. control: **$p < .01$, ***$p < .001$. **(H)** Cumulative probability of c-fos fluorescence intensity in BLA→dmPFC PNs. Kolmogorov-Smirnov test vs. control: ARS (2 hours), $p < .001$; ARS (24 hours), $p = .274$; CRS (2 hours), $p = .096$; CRS (24 hours), $p = .273$. **(I)** Average c-fos fluorescent intensity in BLA→dmPFC PNs. One-way ANOVA; $F_{4,20} = 13.38$, $p < .001$; Bonferroni post hoc comparison vs. control, ***$p < .001$. **(J)** Cumulative probability of c-fos fluorescence intensity in BLA↛dmPFC PNs. Kolmogorov-Smirnov test vs. control: ARS (2 hours), $p < .001$; ARS (24 hours), $p = .164$; CRS (2 hours), $p = .001$; CRS (24 hours), $p = .001$. **(K)** Average c-fos fluorescent intensity in BLA↛dmPFC PNs. One-way ANOVA; $F_{4,20} = 17.07$, $p < .001$; Bonferroni post hoc comparison vs. control **$p < .01$, ***$p < .001$. Pooled data are presented as mean ± SEM. a.u., arbitrary units.

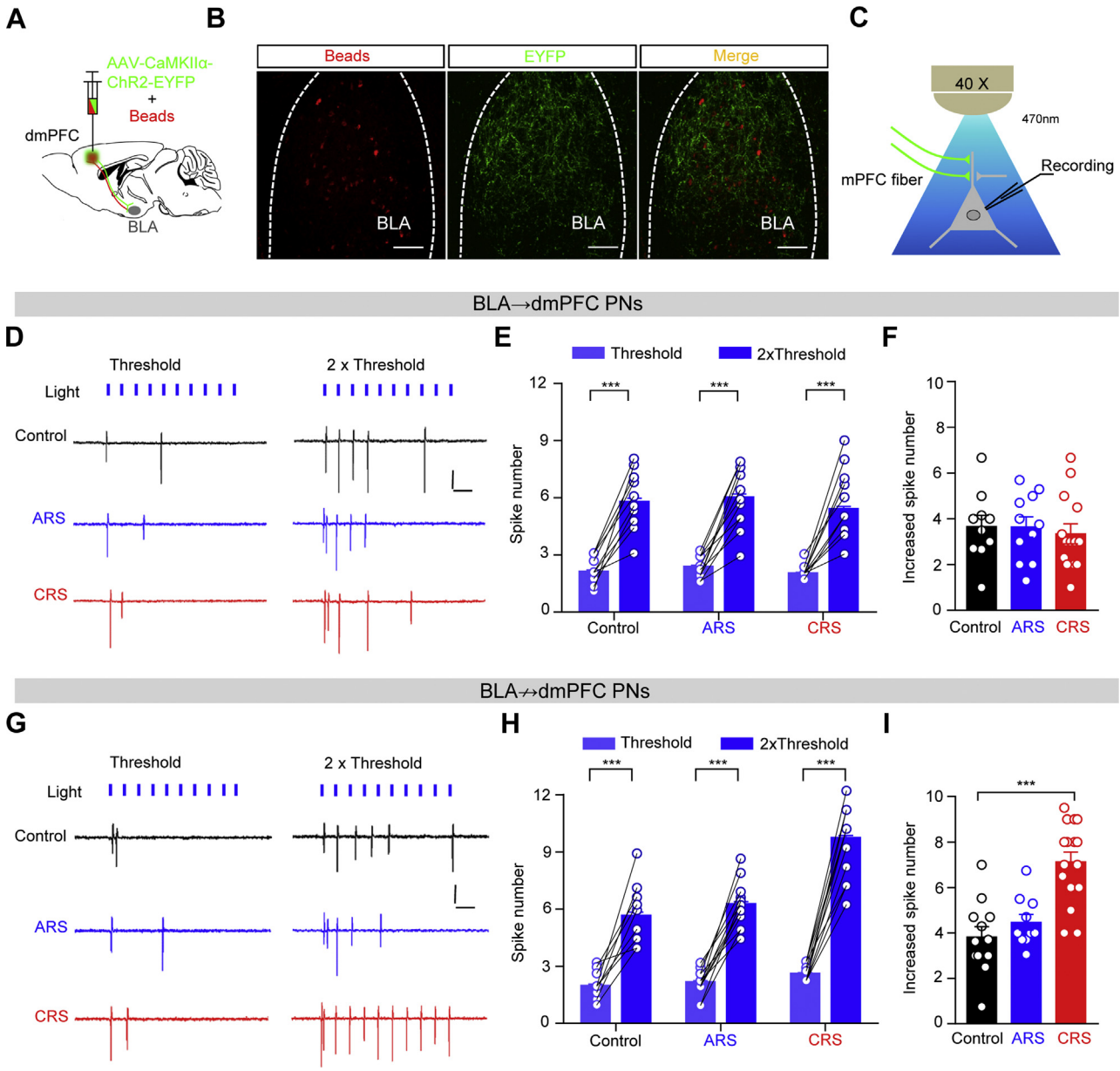

Figure 2. Chronic stress amplifies dorsomedial prefrontal cortex (dmPFC)–induced responses in dmPFC nonprojecting basolateral amygdala (BLA) projection neurons (PNs). **(A)** Injection of adeno-associated virus (AAV) vectors carrying ChR2-EYFP and Retrobeads into dmPFC. **(B)** Representative images showing red Retrobeads labeling (left panel) and channelrhodopsin-2 expression (green, middle panel) in BLA. Representative examples of merged images (right panel). Scale bar = 100 μm. **(C)** Schematic showing optogenetic stimulation of dmPFC afferents to evoke firing of BLA PNs. Neuronal firing was recorded with patch clamp under cell-attached configuration. **(D)** Representative traces showing the firing of BLA→dmPFC PNs when 10 consecutive light stimuli were delivered at 20 Hz. The light intensity was sequentially set at threshold (left) and 2 × threshold value (right). Scale bar = 50 ms, 20 pA. Note that the threshold value varies across recorded cells. **(E)** Summary data showing the changes of spike number in individual BLA→dmPFC PNs (circles) and their mean values (bar) when light intensity was increased, as in panel **(D)**. Control: n = 10 neurons/4 mice; acute restraint stress (ARS): n = 11 neurons/4 mice; chronic restraint stress (CRS): n = 14 neurons/5 mice. Two-way analysis of variance (ANOVA) with repeated measures; main effect of stress treatment: $F_{2,32} = 0.790$, $p = .462$; main effect of light intensity: $F_{1,32} = 179.4$, $p < .001$; interaction: $F_{2,32} = 0.157$, $p = .855$; Bonferroni post hoc comparison, ***$p < .001$. **(F)** Increased spike number in individual BLA→dmPFC PNs (circles) shown in panel **(E)** and their mean values (bar). One-way ANOVA; $F_{2,32} = 0.171$, $p = .844$. **(G)** Firing of BLA↛dmPFC PNs when 10 consecutive light stimuli were delivered at 20 Hz. The light intensity was sequentially increased from threshold (left) and 2 × threshold value (right). Scale bar = 50 ms, 20 pA. **(H)** Summary plots of the changes of spike number in BLA↛dmPFC PNs. Control: n = 12 neurons/4 mice; ARS, n = 10 neurons/4 mice; CRS, n = 16 neurons/5 mice. Two-way ANOVA with repeated measures; main effect of stress treatment: $F_{2,35} = 22.72$, $p < .001$; main effect of light intensity: $F_{1,35} = 343.7$, $p < .001$; interaction: $F_{2,32} = 18.37$, $p < .001$; Bonferroni post hoc comparison, ***$p < .001$. **(I)** Increased spike number in individual BLA↛dmPFC PNs (circles) shown in panel **(H)** and their mean values (bar). One-way ANOVA; $F_{2,35} = 17.730$, $p < .001$; Bonferroni post hoc comparison, ***$p < .001$. Pooled data are presented as mean ± SEM. EYFP, enhanced yellow fluorescent protein.

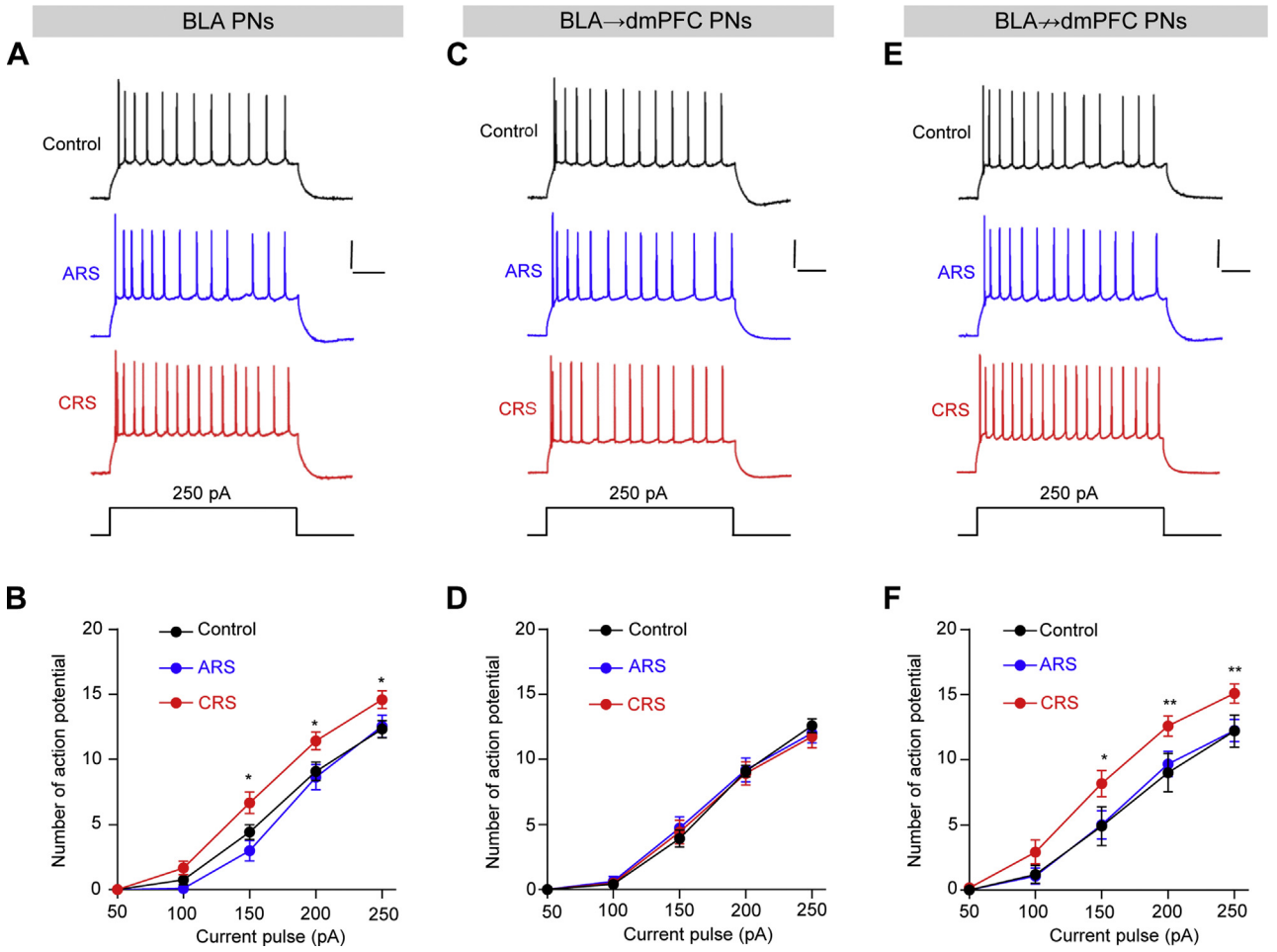

Figure 3. Chronic stress increases excitability in dorsomedial prefrontal cortex (dmPFC) nonprojecting basolateral amygdala (BLA) projection neurons (PNs). **(A)** Representative traces showing the firing of randomly selected BLA PNs in response to current injections (250 pA, 600 ms). Scale bar = 200 ms, 30 mV. **(B)** Summary plots of the action potential number as a function of the injected current strength, as in panel **(A)**. Control: n = 12 neurons/4 mice; acute restraint stress (ARS): n = 12 neurons/4 mice; chronic restraint stress (CRS): n = 12 neurons/4 mice. Two-way analysis of variance with repeated measures; main effect of stress treatment: $F_{2,33} = 5.223$, $p = .01$; main effect of current injection: $F_{4,132} = 435.3$, $p < .001$; interaction: $F_{8,132} = 2.542$, $p = .013$; Bonferroni post hoc comparison, CRS vs. control, $^{*}p < .05$. **(C, D)** Effects of ARS and CRS on the excitability of BLA→dmPFC PNs. Other illustrations as in panels **(A, B)**. Control: n = 12 neurons/4 mice; ARS, n = 11 neurons/4 mice; CRS, n = 12 neurons/4 mice. Two-way analysis of variance with repeated measures; main effect of stress treatment: $F_{2,32} = 0.048$, $p = .953$; main effect of current injection: $F_{4,128} = 350.5$, $p < .001$; interaction: $F_{8,128} = 0.352$, $p = .944$. **(E, F)** Effects of ARS and CRS on the excitability of BLA↛dmPFC PNs. Other illustrations as in panels **(A, B)**. Control: n = 11 neurons/4 mice; ARS: n = 12 neurons/4 mice; CRS: n = 12 neurons/4 mice. Two-way analysis of variance with repeated measures; main effect of stress treatment: $F_{2,32} = 8.883$, $p < .001$; main effect of current injection: $F_{4,128} = 288$, $p < .001$; interaction: $F_{8,128} = 1.516$, $p = .158$; Bonferroni post hoc comparison, CRS vs. control, $^{*}p < .05$, $^{**}p < .01$. Pooled data are presented as mean ± SEM.

designed by Obio Technology (Shanghai, China) and are described in Supplemental Methods.

Statistical Analysis

Statistical analyses were performed using GraphPad Prism (GraphPad Software, Inc., San Diego, CA). Data were analyzed using Student's t test (for two groups) or one-way or two-way analysis of variance with or without repeated measures, followed by post hoc comparisons with the Bonferroni t test. The distribution of c-fos expression in BLA PNs was analyzed with the Kolmogorov-Smirnov comparison. The homoscedasticity and normality of the distributions were analyzed with Bartlett's test and the Kolmogorov-Smirnov test, respectively. Data are presented as mean ± SEM. The threshold for statistical significance was $p < .05$.

RESULTS

Lasting c-fos Activation in BLA↛dmPFC PNs After Chronic Stress

We first compared the topographical organization and collateralization of BLA PNs projecting to the dmPFC relative to PNs projecting to the vHPC, the central amygdala (CeA), or the lower portion of the dorsal striatum by injecting red fluorescent Retrobeads into the dmPFC and green fluorescent Retrobeads into one of these three other regions. This revealed a salt-and-pepper

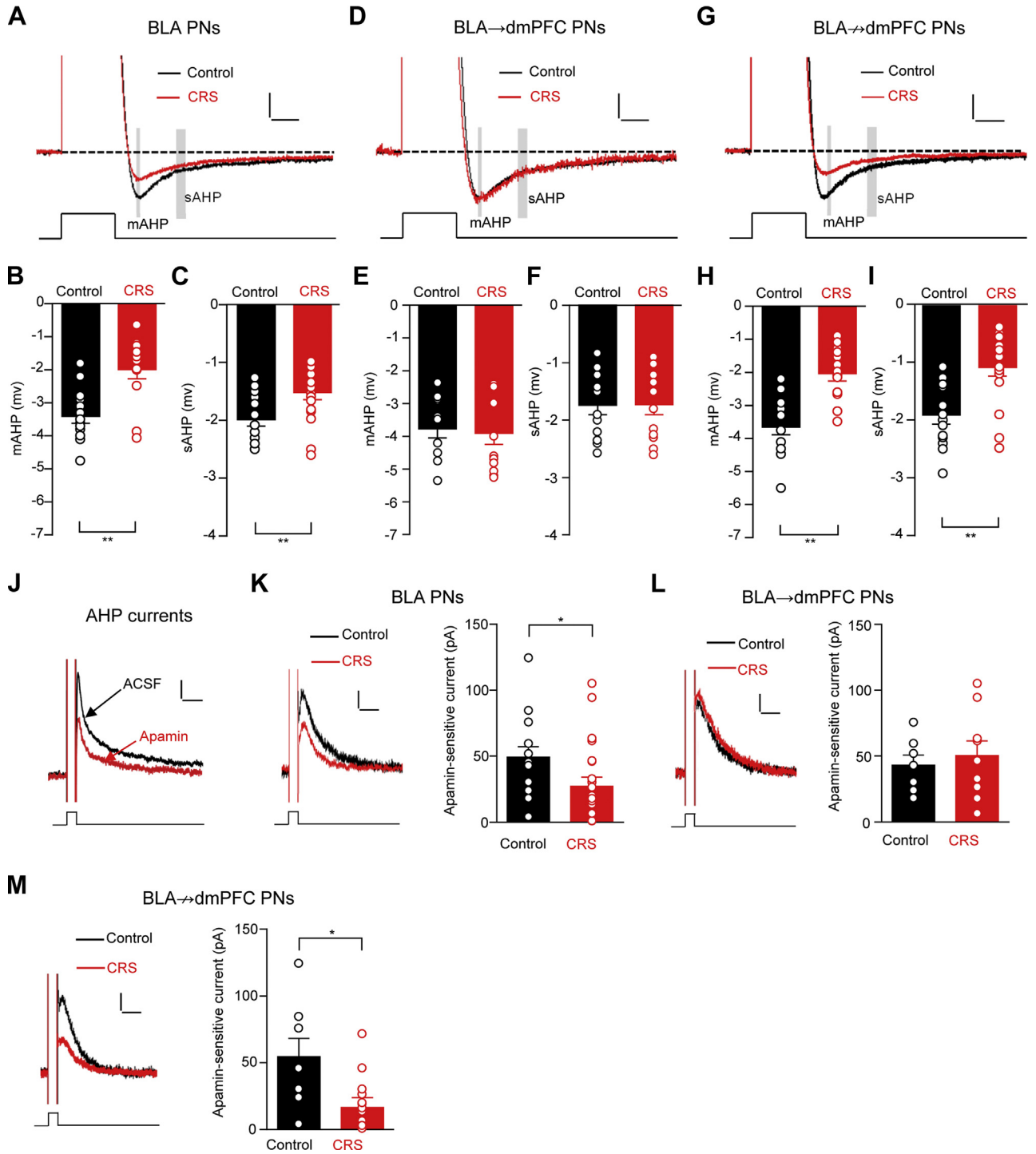

Figure 4. Chronic restraint stress (CRS) reduces small-conductance, calcium-activated potassium channel currents in dorsomedial prefrontal cortex (dmPFC) nonprojecting basolateral amygdala (BLA) projection neurons (PNs). **(A)** Representative traces showing afterhyperpolarization (AHP) evoked by injection of depolarization current pulse. For clarity, the action potentials during current injection were artificially truncated. Scale bar = 100 ms, 2 mV. Medium AHP (mAHP) and slow AHP (sAHP) are indicated by gray bars. **(B, C)** Summary data showing mAHP **(B)** and sAHP **(C)**. Control: n = 14 neurons/4 mice; CRS: n = 13 neurons/5 mice. Two-tailed unpaired t test, $^{**}p < .01$. **(D–F)** Effect of CRS on the mAHP **(E)** and sAHP **(F)** of BLA→dmPFC PNs. Control: n = 12 neurons/4 mice; CRS: n = 12 neurons/5 mice. Scale bar = 100 ms, 2 mV. **(G–I)** Effect of CRS on the mAHP **(H)** and sAHP **(I)** of BLA↛dmPFC PNs. Control: n = 14 neurons/4 mice; CRS: n = 14 neurons/5 mice. Two-tailed unpaired t test, $^{**}p < .01$. Scale bar = 100 ms, 2 mV. **(J)** Representative traces showing AHP currents produced by applying 100-ms voltage step to +45 mV before and after apamin application. Scale bar = 200 ms, 30 pA. **(K)** (Left panel) Representative traces showing apamin-sensitive small-conductance, calcium-activated potassium channel currents in randomly selected BLA PNs. Traces were constructed

distribution of the different PN projectors, with very few somata overlapping (Supplemental Figure S1). This observation is consistent with recent data showing minimal collateralization of PFC projecting and PFC nonprojecting PNs (16).

We next examined whether dmPFC projecting (BLA→dmPFC) PNs and dmPFC nonprojecting (BLA↛dmPFC) PNs responded differently to stress. We injected red fluorescent Retrobeads into the dmPFC and later subjected mice to either 1 day of 2-hour ARS or 10 consecutive days of 2-hour CRS (Figure 1A–C), followed by 2-hour or 24-hour stress-free recovery. ARS increased the number of c-fos$^+$ cells in the BLA 2 hours, but not 1 day, later, compared with unstressed controls and with no difference between Retrobead labeled (BLA→dmPFC) and unlabeled (putative BLA↛dmPFC) PNs (Figure 1D, E). The same pattern of effects was evident when the fluorescence intensity of c-fos labeling was used as the dependent measure (Figure 1F–K).

In contrast to ARS, CRS produced an increase in c-fos$^+$ labeling that was evident not only 2 hours but also 24 hours later and only in Retrobead-unlabeled, putative BLA↛dmPFC PNs. This effect was similar regardless of whether the number of c-fos$^+$ cells or c-fos labeling fluorescence intensity within the imaged region of interest was quantified (Figure 1D–K). These results indicate that after a regimen of CRS, but not ARS, neuronal activation in BLA→dmPFC PNs returns to baseline within 1 day, but neighboring putative BLA↛dmPFC PNs remain persistently activated.

Increased Firing to dmPFC Input in BLA↛dmPFC PNs After Chronic Stress

To establish a physiological correlate of the persistent CRS-induced increase in c-fos expression in BLA↛dmPFC PNs, we next explored how the two populations fire to synaptic inputs after ARS or CRS. BLA receives afferents from multiple brain regions, and, among them, afferents from mPFC preferentially innervate BLA rather than its neighboring lateral amygdala or CeA (27). We thus selected dmPFC as a target input region of BLA.

After transfecting dmPFC PNs with the light-sensitive opsin, channelrhodopsin-2 (Figure 2A, B), fibers in the BLA were photoactivated, and the firing of BLA→dmPFC PNs and BLA↛dmPFC PNs was recorded under a cell-attached patch clamp configuration (Figure 2C). To reduce variation in firing resulting from varying channelrhodopsin-2 expression across mice, light intensity was adjusted for each recorded PN to a threshold level producing one to three spikes on 10 consecutive stimuli (2 ms, 20 Hz), then doubled to determine the increase in spike number as an indication of BLA neuronal responsiveness to dmPFC activation (Figure 2D–I).

One day after either ARS or CRS, the firing BLA→dmPFC PNs to dmPFC input photoactivation was not different from unstressed control subjects (Figure 2D–F). Conversely, photoactivation produced a significantly greater increase in BLA↛dmPFC PN firing 1 day after CRS, but not ARS, relative to unstressed control subjects (Figure 2G–I). This finding complements the c-fos activation data by indicating a persistent and selective increase in the firing of putative BLA↛dmPFC PNs after CRS.

Increased Intrinsic Excitability in BLA↛dmPFC PNs After Chronic Stress

Plastic regulation of neuronal intrinsic excitability represents an important mechanism via which the brain cells adapt to the changing environment. Therefore, we next explored whether CRS differentially affected the intrinsic excitability of BLA→dmPFC PNs and BLA↛dmPFC PNs.

ARS failed to affect the excitability of BLA PNs when they were either randomly selected or separated based on whether they project to dmPFC. By contrast, CRS significantly increased the excitability of BLA PNs (Figure 3A, B) only in the BLA↛dmPFC subpopulation (Figure 3C–F)—thereby indicating projection-specific regulation of CRS on the excitability of BLA PNs. As our findings indicated population-wide recovery of BLA PNs from ARS, in terms of their c-fos expression, firing to dmPFC inputs, and intrinsic excitability, we investigated only the effects of CRS in the remaining experiments.

Hyperexcitability in BLA↛dmPFC PNs Is Associated With Asymmetric SK Channel Alterations

The finding that CRS preferentially increases neuronal excitability in BLA↛dmPFC PNs, but not BLA→dmPFC PNs, next led us to consider potential mechanisms that might underlie this. Among the diverse factors regulating neuronal excitability, the calcium-activated potassium channel family plays a central role. To study the potential involvement of calcium-activated potassium channels in CRS-related excitability, we measured the fast and medium components of afterhyperpolarization (AHP): voltage signatures of large-conductance, calcium-activated potassium channels and SK channels, respectively.

CRS did not alter fast AHP of BLA PNs, regardless of projections to the dmPFC (Supplemental Figure S2A–F). Isolating the large-conductance, calcium-activated potassium channel current with the selective large-conductance, calcium-activated potassium channel blocker tetraethylammonium also revealed no significant changes following CRS (Supplemental Figure S2G–L). By contrast, CRS markedly reduced medium AHP (mAHP), but only in BLA↛dmPFC PNs (Figure 4A–I). Blocking SK channel currents using the selective blocker apamin yielded similar findings (Figure 4J–M). CRS also reduced slow AHP in BLA↛dmPFC PNs, but not BLA→dmPFC PNs (Figure 4A–I). These findings indicate an effect of CRS on SK channel function restricted to BLA↛dmPFC PNs.

by subtracting the currents in the presence of apamin from the currents in its absence. Scale bar = 200 ms, 15 pA. (Right panel) Summary plot showing the apamin-sensitive currents (circles) and their mean value (bar). Control: n = 15 neurons/5 mice; CRS: n = 22 neurons/6 mice. Two-tailed unpaired t test, $^*p < .05$. **(L)** Effect of CRS on apamin-sensitive current in BLA→dmPFC PNs. Control: n = 7 neurons/5 mice; CRS: n = 9 neurons/6 mice. Scale bar = 200 ms, 15 pA. **(M)** Effect of CRS on apamin-sensitive current in BLA↛dmPFC PNs. Control: n = 8 neurons/6 mice; CRS: n = 13 neurons/6 mice. Two-tailed unpaired t test, $^*p < .05$. Scale bar = 200 ms, 15 pA. Pooled data are presented as mean ± SEM. ACSF, artificial cerebrospinal fluid.

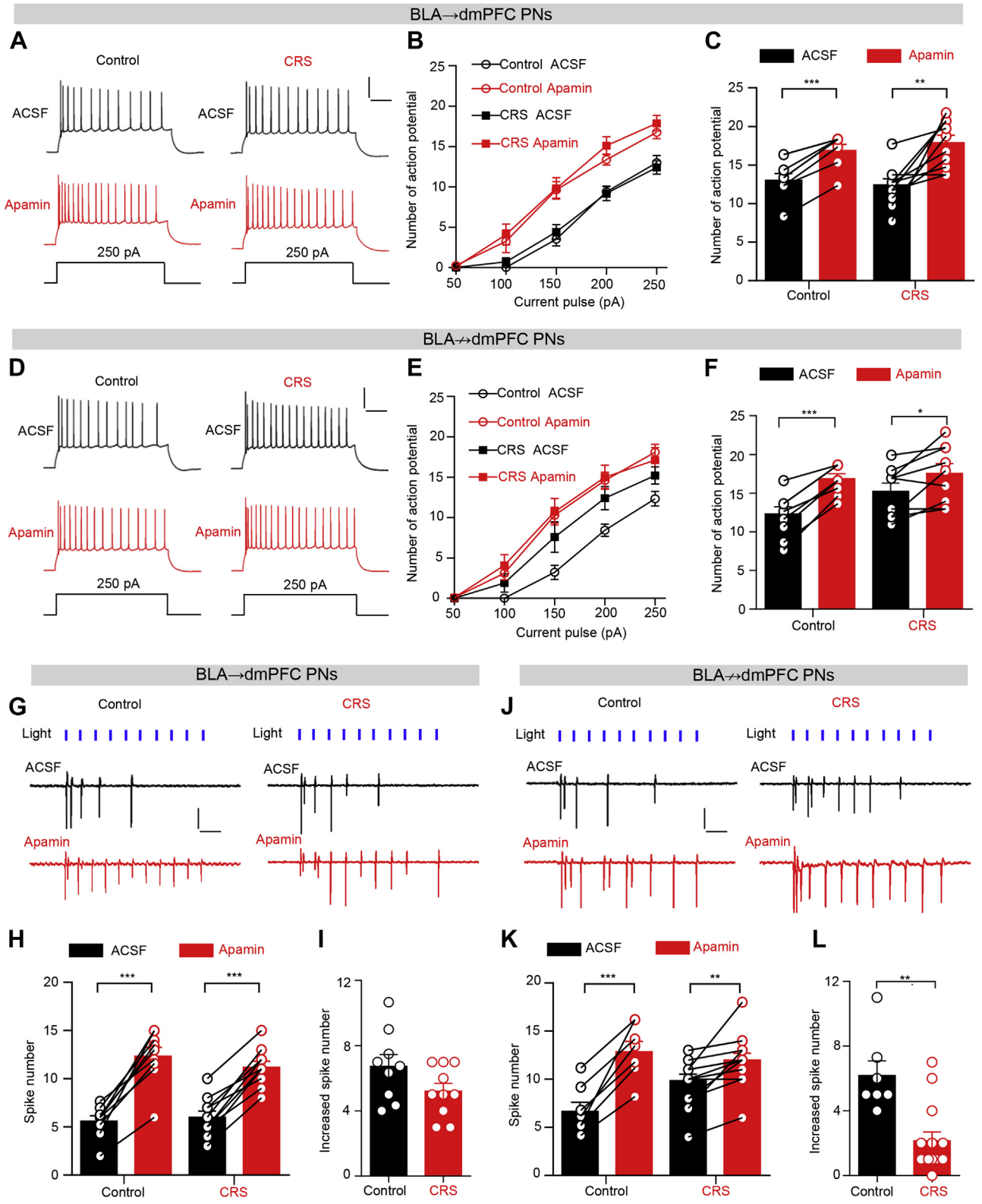

Figure 5. Small-conductance, calcium-activated potassium channel blockade abolishes stress-induced increases in excitability in dorsomedial prefrontal cortex (dmPFC) nonprojecting basolateral amygdala (BLA) projection neurons (PNs). **(A)** Representative traces showing the firing of BLA→dmPFC PNs on injection of a depolarizing current (bottom panel) when slices were successively perfused with artificial cerebrospinal fluid (ACSF) and apamin. Scale bar = 200 ms,

We examined the influence of CRS on other factors involved in the regulation of neuronal excitability. As shown in Supplemental Table S1, CRS had little influence on resting membrane potential, input resistance, and firing threshold of BLA PNs, and these effects were independent of output targets, suggesting minimal contribution to CRS-induced increase of neuronal excitability.

Next, to ascertain whether asymmetric alterations in SK channel currents in the two BLA PN output populations account for their different adaptation to CRS, we examined the influence of apamin on their intrinsic excitability. Apamin similarly increased the excitability of BLA→dmPFC PNs from both control and CRS mice but had a weaker effect in BLA↛dmPFC PNs of the CRS group relative to the unstressed control subjects (Figure 5A–F). Apamin also differentially affected the firing of the two populations to dmPFC inputs: increasing the firing of BLA→dmPFC PNs similarly from unstressed control and CRS mice, but increasing firing in BLA↛dmPFC PNs only in the control mice and not the CRS mice (Figure 5G–L).

In sum, these results suggest that the asymmetric SK channel alterations represent a plausible mechanism underlying the different responses to CRS in the two PN populations.

SK Channel Downregulation in BLA↛dmPFC PNs Correlates With Anxiety-like Behavior

Emotional disturbances, such as heightened anxiety, that result from chronic stress are linked to hyperactivation of amygdala neurons (28). We next sought to determine whether there was a relationship between loss of SK channel function (and the associated hyperactivation of BLA↛dmPFC PNs seen after CRS) and anxiety-like behavior. Anxiety-like behavior was measured after CRS in the elevated plus maze (EPM) and novel open field test (OFT), and AHP measurements were then done in the same mice 4 hours later (Figure 6A). Relative to unstressed control subjects, the CRS group exhibited increased anxiety-like behavior, as indicated by less time spent and fewer entries into the open arms of the EPM (Figure 6B–D) and less time spent in the center of the OFT apparatus (Figure 6E–G).

Subsequent neuronal recordings replicated our earlier observation of a reduction in mAHP in BLA↛dmPFC PNs, but not BLA→dmPFC PNs, following CRS (Supplemental Figure S3). In unstressed control mice, there were no significant correlations between mean AHP (averaged from three to five cells for each mouse) and measures of anxiety-like behavior for either PN population (Figure 6H, I, L, M). In CRS mice, however, these measures were significantly and inversely correlated with the magnitude of mAHP in BLA↛dmPFC PNs, but not BLA→dmPFC PNs (Figure 6J, K, N, O). For both stressed and control mice, there were no significant correlations between anxiety-like behavior and slow AHP (Supplemental Figure S4). These data therefore support a link between loss of SK channel currents in BLA↛dmPFC PNs and CRS-related increases in anxiety-like behavior.

SK2 Channel Downregulation in BLA↛dmPFC PNs After Chronic Stress

As apamin blocks both SK2 and SK3 channels, the reduction in apamin-sensitive currents we observed after CRS may arise from the desensitization of either one of the channel subtypes or both channel subtypes. Therefore, we next sought to identify the SK channel subtypes affected by CRS, using Lei-Dab7 to selectively block SK2 (29). Relative to unstressed controls, CRS mice had weaker Lei-Dab7-sensitive SK2 channel currents in BLA↛dmPFC PNs, but not BLA→dmPFC PNs (Supplemental Figure S5). Moreover, in the presence of Lei-Dab7, application of apamin had negligible influence on the recorded currents in either PN population (data not shown), consistent with the weak expression of SK3 channel in BLA (30). These data suggest that the SK2 channel subtype underlies the loss of SK channel function in BLA↛dmPFC PNs after CRS.

SK2 Channel Overexpression in BLA↛dmPFC PNs Prevents CRS-Induced Hyperexcitability and Anxiety-like Behavior

We next tested for a causal link between loss of SK2 channel function in BLA↛dmPFC PNs and CRS-induced anxiety by testing whether selectively preventing SK downregulation in these cells protected against the effects of CRS. The SK2 channel was expressed in BLA↛dmPFC PNs by injecting a

30 mV. **(B)** Summary plots showing the number of action potentials against the injected current strength. Control: n = 8 neurons/4 mice; chronic restraint stress (CRS): n = 10 neurons/4 mice. Two-way analysis of variance with repeated measures; control mice, main effect of apamin: $F_{1,7} = 27.51$, $p = .001$; control mice, main effect of current injection: $F_{4,28} = 164.9$, $p < .001$; control mice, interaction: $F_{4,28} = 7.878$, $p < .001$; CRS mice, main effect of apamin: $F_{1,9} = 17.87$, $p = .002$, CRS mice, main effect of current injection: $F_{4,36} = 152.6$, $p < .001$; CRS mice, interaction: $F_{4,36} = 6.886$, $p < .001$. **(C)** Apamin-induced changes of action potential number in individual BLA→dmPFC PNs (circles) and their mean values (bar) when the current strength was set at 250 pA. Two-tailed paired t test, $^{**}p < .01$; $^{***}p < .001$. **(D)** Same as in panel **(A)** except that the data were from BLA↛dmPFC PNs. Scale bar = 200 ms, 30 mV. **(E)** Plot of firing of BLA↛dmPFC PNs against the strength of injected currents. Control: n = 10 neurons/4 mice; CRS: n = 10 neurons/4 mice. Two-way analysis of variance with repeated measures: control mice, main effect of apamin: $F_{1,9} = 105.5$, $p < .001$; control mice, main effect of current injection: $F_{4,36} = 214.7$, $p < .0001$; control mice, interaction: $F_{4,36} = 24.62$, $p < .0001$; CRS mice, main effect of apamin: $F_{1,9} = 17.941$, $p = .002$; CRS mice, main effect of current injection: $F_{4,36} = 109.1$, $p < .001$; CRS mice, interaction: $F_{4,36} = 3.606$, $p = .014$. **(F)** Apamin-induced changes of action potential number in individual BLA↛dmPFC PNs (circles) and the mean (bar) when current strength was set at 250 pA. Two-tailed paired t test, $^{*}p < .05$; $^{***}p < .001$. **(G)** Representative traces showing the firing of BLA→dmPFC PNs when 10 consecutive light stimuli were delivered. The light intensity was set at 2 × threshold. Cell firing was sequentially recorded in the absence (top panel) or presence (bottom panel) of apamin. Scale bar = 50 ms, 20 pA. **(H)** Summary plots of the spike number in individual BLA→dmPFC PNs (circles) and their mean value (bar). Control: n = 9 neurons/4 mice; CRS: n = 10 neurons/4 mice. Two-tailed paired t test, $^{***}p < .001$. **(I)** Apamin-induced increase in the spike number of individual BLA→dmPFC PNs (circles) and their mean value (bar). Two-tailed paired t test, $p = .193$. **(J)** Same as in panel **(G)** except data are from BLA↛dmPFC PNs. Scale bar = 50 ms, 20 pA. **(K)** Summary of data shown in panel **(J)**. Control: n = 7 neurons/3 mice; CRS mice: n = 14 neurons/5 mice. Note that some pairs have the same spike number before and after apamin application and are therefore overlapped. Two-tailed paired t test, $^{**}p < .01$, $^{***}p < .001$. **(L)** Apamin-induced increase in spike number of BLA↛dmPFC PNs. Two-tailed unpaired t test, $^{**}p < .01$. Pooled data are presented as mean ± SEM.

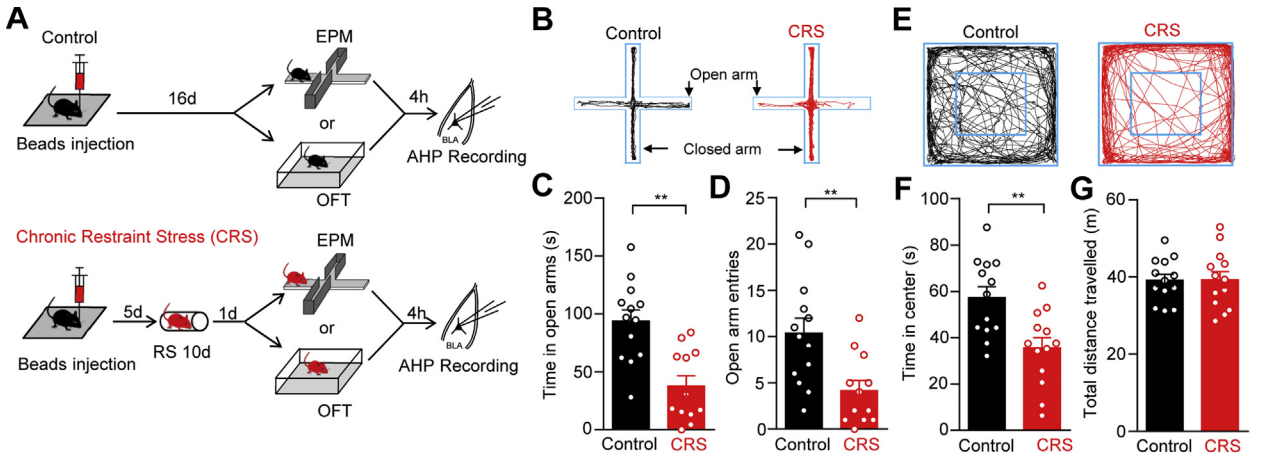

Control mice-EPM

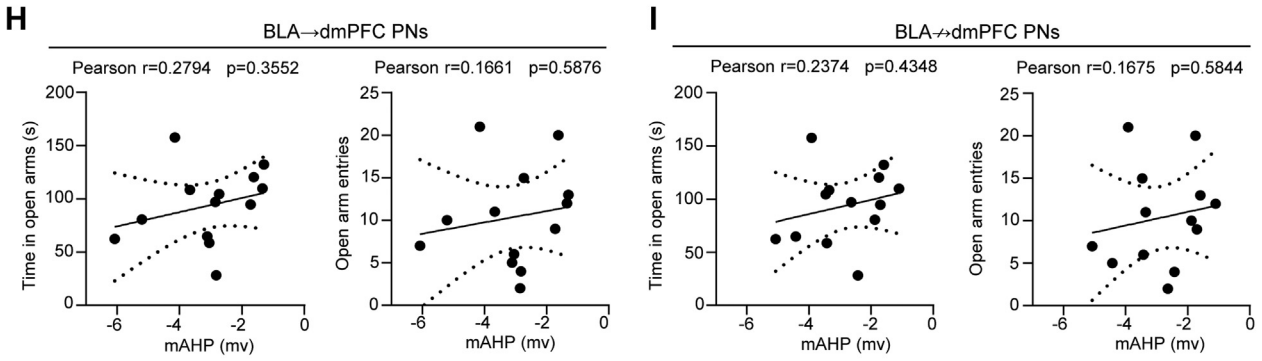

CRS mice-EPM

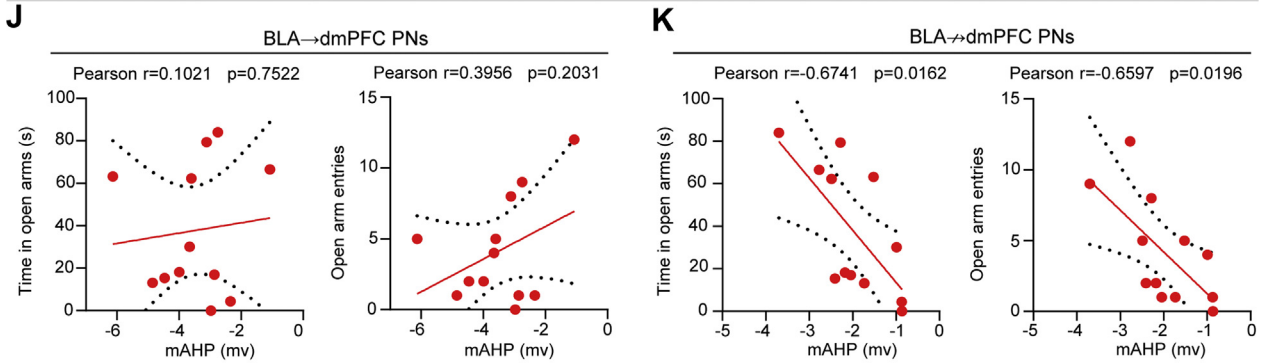

Control mice-OFT

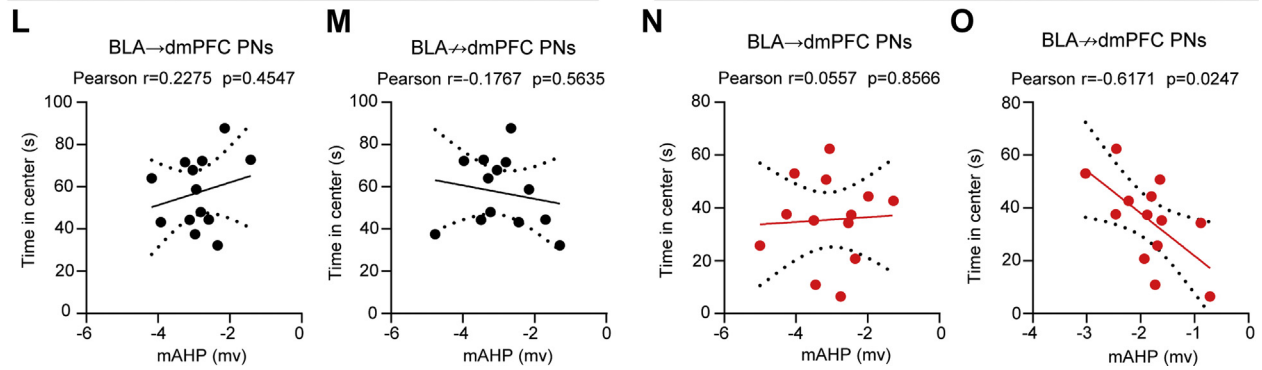

CRS mice-OFT

double-floxed, Cre-dependent AAV vector expressing SK2 fused with fluorescent protein mCherry (AAV-DO-SK2-mCherry) into the BLA (SK2-mCherry group), along with a retrogradely traveling AAV vector expressing Cre-recombinase fused with enhanced yellow fluorescent protein (AAV-retro-EYFP-Cre) into the dmPFC (Figure 7A–C). Injection of the retrograde AAV helper vector rAAV-retro into dmPFC results in the retrograde transportation of EYFP-Cre to cell bodies of BLA→dmPFC PNs, where it drives expression of Cre recombinase preventing SK2 channel gene expression. A control AAV vector expressing mCherry, but not SK2, was injected into the BLA of a control group (mCherry-only group).

To first validate the efficacy and specificity of this viral strategy for enhancing SK channel function in BLA↛dmPFC PNs, we compared mAHP in SK2-mCherry and mCherry-only. mAHP of the nontransfected BLA→dmPFC PNs was comparable between the two groups (Supplemental Figure S6). By contrast, mAHP in BLA↛dmPFC PNs was higher in the SK2-mCherry group. No changes in slow AHP were observed in either PN population.

We next found that in both the SK2-mCherry and the mCherry-only groups, CRS had little influence on mAHP of BLA→dmPFC PNs (Figure 7D, E). By contrast, CRS markedly reduced mAHP of BLA↛dmPFC PNs in mCherry-only group but only slightly reduced mAHP in SK2-mCherry mice (Figure 7F, G). After CRS, mAHP of BLA↛dmPFC PNs in the SK2-mCherry group was higher than in the mCherry-only group, showing that genetic introduction of SK2 to BLA↛dmPFC PNs was effective in preventing CRS-induced loss of SK channel function in this population. Moreover, the viral manipulation had little influence on the excitability of BLA→dmPFC PNs from either control or CRS mice, but it occluded the increased excitability of BLA↛dmPFC PNs by CRS (Figure 7H–K).

We went on to examine whether SK2 channel expression in BLA↛dmPFC PNs affected CRS-induced anxiety-like behavior. Under unstressed conditions, the mCherry-only and SK2-mCherry groups did not differ in EPM and OFT behavior, whereas CRS increased anxiety-like behavior in the mCherry-only mice but failed to do so in the SK2-mCherry group (Figure 7L–Q). Thus, in addition to protecting against CRS-induced loss of SK channel function in BLA↛dmPFC PNs, virus-mediated expression of SK2 channel in this PN population was sufficient to prevent the anxiety-related sequelae of CRS.

SK Channel Downregulation in vHPC-Projecting BLA PNs After Chronic Stress Is Associated With Anxiety-like Behavior

Given that BLA↛dmPFC PNs have diverse projection targets, our findings thus far did not identify the specific PN output population affected by CRS. To address this issue, we selected two subpopulations of BLA PNs targeting either the vHPC (BLA→vHPC PNs) or the NAc (BLA→NAc PNs), which have been reported to encode anxiety and reward, respectively (20,21,31). The two populations were identified by red and green fluorescent retrogradely transported beads, respectively. The somata of these two neuronal subsets had little overlap in the BLA (Figure 8A–C).

We found that CRS robustly increased the excitability of BLA→vHPC PNs but had little effect on BLA→NAc PNs (Figure 8D, E) and, likewise, decreased mAHP only in the former population (Figure 8F, G). These projection-specific effects also accounted for behavioral effects of CRS to the extent that the magnitude of mAHP in BLA→vHPC PNs positively correlated with EPM and OFT anxiety-like behaviors (Figure 8H–K).

SK2 Channel Overexpression in BLA→vHPC PNs Prevents CRS-Induced Anxiety-like Behavior

Finally, to substantiate the relationship between SK channel loss in BLA→vHPC PNs and anxiety-like behavior, we employed another intersectional viral strategy to selectively express SK2 channel in BLA→vHPC PNs. The SK2 channel was expressed in BLA→vHPC PNs by injecting a retrogradely traveling AAV vector expressing Cre-recombinase fused with enhanced yellow fluorescent protein ($AAV_{2/1}$-retro-*Syn*-EYFP-Cre) into the vHPC, along with a Cre-dependent vector expressing SK2 fused with fluorescent protein mCherry ($AAV_{2/8}$-*CaMKIIα*-DIO-SK2-mCherry) into the BLA (SK2-mCherry group) or an $AAV_{2/8}$-CaMKIIα-DIO-mCherry control (mCherry-only) (Figure 8L–N). Injection of rAAV-retro into vHPC results in the retrograde transportation of EYFP-Cre to the BLA, where it drives SK2 channel gene expression in BLA→vHPC PNs.

Behavioral testing demonstrated that the mCherry-only and SK2-mCherry groups did not differ in the EPM and OFT tests; however, whereas CRS increased anxiety-like behavior in the mCherry-only mice, it did not do so in the SK2-mCherry group (Figure 8O–Q). These data identify BLA→vHPC PNs as at least one key output pathway underlying CRS-induced SK channel downregulation and the associated increase in anxiety-like behavior.

DISCUSSION

In this article, we provide novel evidence that BLA PNs exhibit highly divergent patterns of neuroadaptation to chronic stress depending on their extra-amygdala projection targets. Specifically, we found that BLA PNs show rapid recruitment and recovery following acute stress exposure, regardless of

Figure 6. Stress-induced anxiety-like behavior is associated with medium afterhyperpolarization (mAHP) magnitude in dorsomedial prefrontal cortex (dmPFC) nonprojecting basolateral amygdala (BLA) projection neurons (PNs). **(A)** Schematic showing the experimental procedures for unstressed control mice and chronic restraint stress (CRS) mice. **(B)** Representative activity tracking in the elevated plus maze (EPM) in control and CRS mice. **(C)** EPM open arm time. Control mice, $n = 13$; CRS mice, $n = 12$. Two-tailed unpaired t test, $^{**}p < .01$. **(D)** EPM open arm entries. Same sample size as in panel **(C)**. Two-tailed unpaired t test, $^{**}p < .01$. **(E)** Representative activity tracking in the open field test (OFT) in control and CRS mice. **(F)** OFT center time. Control mice, $n = 13$; CRS mice, $n = 13$. Two-tailed unpaired t test, $^{**}p < .01$. **(G)** OFT total distance traveled. Same sample size as in panel **(F)**. Two-tailed unpaired t test, $^{**}p < .01$. **(H, I)** Correlations between mAHP in BLA→dmPFC PNs **(H)** and BLA↛dmPFC PNs **(I)** and open arm time and entries in control mice. **(J, K)** Correlations between mAHP in BLA→dmPFC PNs **(J)** and BLA↛dmPFC PNs **(K)** and open arm time and entries in CRS mice. **(L, M)** Correlations between mAHP in BLA→dmPFC PNs **(L)** and BLA↛dmPFC PNs **(M)** and the time control mice spent in center. **(N, O)** Correlations between mAHP in BLA→dmPFC PNs **(N)** and BLA↛dmPFC PNs **(O)** and time CRS mice spent in center. Pooled data are presented as mean ± SEM.

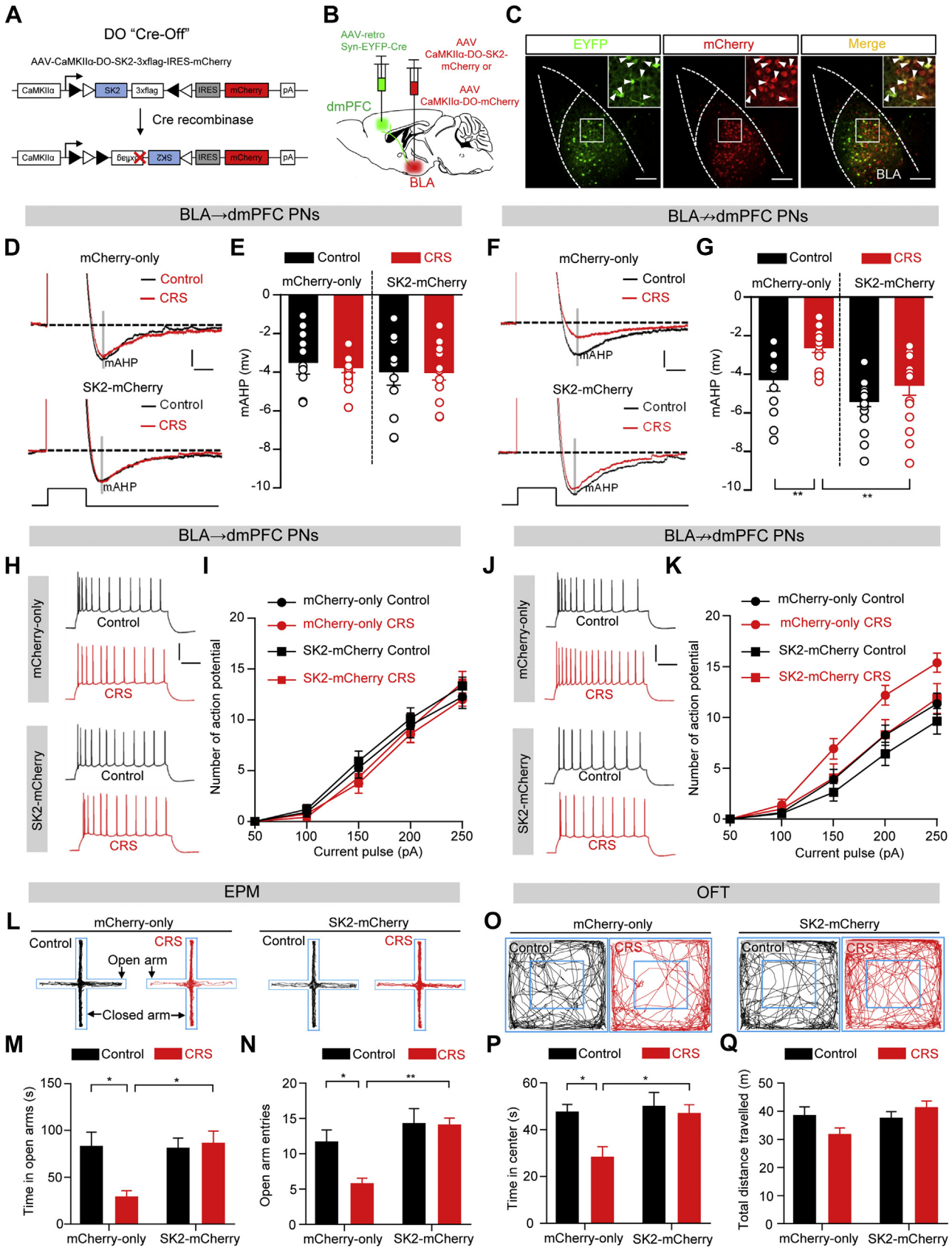
A
DO "Cre-Off"
AAV-CaMKIIα-DO-SK2-3xflag-IRES-mCherry
CaMKIIα
SK2
3xflag
IRES
mCherry
pA
Cre recombinase
B
AAV-retro Syn-EYFP-Cre
AAV CaMKIIα-DO-SK2-mCherry or
AAV CaMKIIα-DO-mCherry
dmPFC
BLA
C
EYFP
mCherry
Merge
BLA
BLA→dmPFC PNs
BLA↛dmPFC PNs
D
mCherry-only
Control
CRS
mAHP
SK2-mCherry
E
Control
CRS
mCherry-only
SK2-mCherry
mAHP (mv)
F
G
**
H
I
mCherry-only Control
mCherry-only CRS
SK2-mCherry Control
SK2-mCherry CRS
Number of action potential
Current pulse (pA)
J
K
EPM
OFT
L
Open arm
Closed arm
O
M
Time in open arms (s)
N
Open arm entries
P
Time in center (s)
Q
Total distance travelled (m)

whether they targeted dmPFC, but that exposure to chronic stress causes persistent activation and hyperexcitability in PNs that do not project to the dmPFC—which we then went on to identify as vHPC projectors. Mechanistically, we link these projection-specific changes to a downregulation of SK2 subtype function and show that selectively preventing this adaptation is sufficient to prevent chronic stress-induced neuronal excitability and anxiety-like behavior.

The amygdala has long known been known to be one of the primary neural targets of stress and mediates many aspects of stress-related physiology and pathology (4,11). Similar to earlier findings that acute stress exposure caused immediate but temporary activation of amygdala neurons (32), we observed that the c-fos expression in BLA PNs and their intrinsic excitability and firing to dmPFC inputs returned to baseline 1 day after ARS. BLA→dmPFC PNs and BLA↛dmPFC PNs showed equivalent habituation to ARS, extending our recent finding that ARS similarly and temporarily augmented glutamatergic transmission onto these two PN populations (33). Thus, there appears to be minimal divergence in how these populations respond to an intense but short-lasting stressor.

Though BLA PN projections to the PFC are glutamatergic/excitatory, synaptic connections onto interneurons exert strong feedforward inhibition onto cortical neurons (34,35). Consequently, BLA input generally has a net inhibitory effect in PFC (34–36). Thus, ARS recruitment of BLA→dmPFC PNs may inhibit dmPFC activity to temporarily suppress executive functions and bias neural resources to systems critical for the detection and avoidance of threat via, for example, excitatory BLA inputs to subcortical regions, including the vHPC, bed nucleus of the stria terminalis, and CeA (1). Clearly, a system that enables such a parallel shift in neural processing in the presence of acute stress would be of high adaptive value.

Upon chronic stress, BLA PNs have been shown to exhibit enduring changes in terms of their morphology (37), excitability (38), plasticity (39), and crosstalk with other limbic regions and hypothalamic-pituitary-adrenal axis (40,41). Notably, the recruitment of BLA neurons occurs in a highly heterogeneous fashion in various behavioral settings (42–45), which is likely determined by the molecular properties and circuit membership of BLA PNs (16,42,45). For example, BLA→dmPFC PNs and BLA→CeA PNs are engaged in fear and anxiety-related tasks (22,46–48). Consistent with this, we found that CRS produced an enduring increase in c-fos expression, intrinsic excitability, and responsivity to dmPFC input in BLA PNs, but only in those with terminals bypassing the dmPFC. This finding nicely parallels our recent finding that CRS selectively augments glutamatergic transmission onto BLA↛dmPFC PNs and increases the density of mature mushroom-shape spines on these cells (26). It also extends earlier work showing that CRS caused dendritic hypotrophy in mPFC neurons projecting to other cortical regions, but with minimal effects on projections to the BLA (49). Less directly relevant, but still notable in the context of our data, is the finding that chronic social defeat was reported to increase the firing rate of ventral tegmental area neurons projecting to the NAc, but not the mPFC (50).

Taken together, these data raise the intriguing possibility that certain mPFC circuits may be resilient to the effects of chronic stress. On one hand, a higher capacity to maintain the

Figure 7. Protection against stress-induced anxiety-like behavior by prevention of small-conductance, calcium-activated potassium (SK) channel downregulation in dorsomedial prefrontal cortex (dmPFC) nonprojecting basolateral amygdala (BLA) projection neurons (PNs). **(A)** Using Cre-Off strategy to express SK2 channel in BLA↛dmPFC PNs. **(B)** Schematic showing injection of rAAV$_2$-retro-*syn*-EYFP-Cre into dmPFC and AAV$_{2/8}$-*CaMKIIα*-DO-SK2-3xFlag-mCherry or AAV$_{2/8}$-*CaMKIIα*-DO-3xFlag-mCherry into BLA. Injection of rAAV-retro into dmPFC results in the retrograde transportation of EYFP-Cre to cell bodies of BLA→dmPFC PNs, where it drives expression of Cre recombinase preventing SK2 gene expression. **(C)** Representative images showing expression of Cre-recombinase (arrowhead in left panel) and SK2 (arrowhead in middle panel) in BLA neurons. Images are merged in right panel. Note that the vast majority of BLA→dmPFC PNs were transfected by the two vectors. Scale bar = 100 μmol. **(D)** Representative traces showing medium afterhyperpolarization (mAHP) in BLA→dmPFC PNs of mCherry-only and SK2-mCherry mice. The two groups were subjected to injection of AAV$_{2/8}$-*CaMKIIα*-DO-3xFlag-mCherry and AAV$_{2/8}$-*CaMKIIα*-DO-SK2-3xFlag-mCherry, respectively, in BLA. Scale bar = 100 ms, 2 mV. **(E)** Summary of data shown in panel **(D)**. mCherry-only: n = 13 neurons/4 control mice, n = 14 neurons/4 chronic restraint stress (CRS) mice; SK2-mCherry: n = 10 neurons/3 control mice; n = 13 neurons/4 CRS mice. Two-way analysis of variance (ANOVA); main effect of CRS: $F_{1,46}$ = 0.2651, p = .609; main effect of vector injection: $F_{1,46}$ = 2.891, p = .096; interaction: $F_{1,46}$ = 1.302, p = .260. **(F)** Same as in panel **(D)** except that the data are from BLA↛dmPFC PNs. Scale bar = 100 ms, 2 mV. **(G)** Summary of the data shown in panel **(F)**. mCherry-only: n = 10 neurons/4 control mice, n = 14 neurons/4 CRS mice; SK2-mCherry: n = 14 neurons/3 control mice; n = 14 neurons/4 CRS mice. Two-way ANOVA; main effect of CRS: $F_{1,48}$ = 11.12, p = .0017; main effect of vector injection: $F_{1,48}$ = 28.58, $p < .001$; interaction: $F_{1,48}$ = 0.3620, p = .550; Bonferroni post hoc comparison, $^{**}p < .01$. **(H)** Representative traces showing firing of BLA→dmPFC PNs to depolarizing current injection from mCherry-only and SK2-mCherry mice. Scale bar = 200 ms, 30 mV. **(I)** Plot of number of action potentials in BLA→dmPFC PNs against the injected current strength. mCherry-only: n = 11 neurons/4 control mice, n = 11 neurons/4 CRS mice. Two-way ANOVA with repeated measures; main effect of CRS: $F_{1,20}$ = 1.002, p = .329; main effect of current injection: $F_{4,80}$ = 183, $p < .001$; interaction: $F_{4,80}$ = 1.036, p = .3942. SK2-mCherry: n = 15 neurons/5 control mice, n = 12 neurons/4 CRS mice. Two-way ANOVA with repeated measures; main effect of CRS: $F_{1,25}$ = 0.403, p = .531; main effect of current injection: $F_{4,100}$ = 176.1, $p < .001$; interaction: $F_{4,100}$ = 0.7733, p = .5451. **(J)** Same as in panel **(H)** except that the data are from BLA↛dmPFC PNs. Scale bar = 200 ms, 30 mV. **(K)** Summary of data shown in panel **(J)**. mCherry-only: n = 11 neurons/4 control mice; n = 15 neurons/4 CRS mice. Two-way ANOVA; main effect of CRS: $F_{1,24}$ = 6.026, p = .022; SK2-mCherry: n = 14 neurons/4 control mice, n = 16 neurons/4 CRS mice. Two-way ANOVA; main effect of CRS: $F_{1,28}$ = 1.024, p = .320. **(L)** Representative activity tracking in the elevated plus maze (EPM) in mCherry-only and SK2-mCherry mice. **(M)** EPM open arm time. mCherry-only: n = 10 control mice, n = 10 CRS mice; SK2-mCherry: n = 10 control mice, n = 12 CRS mice. Two-way ANOVA; main effect of CRS: $F_{1,38}$ = 3.608, p = .065; main effect of vector injection: $F_{1,38}$ = 4.632, p = .038; interaction: $F_{1,38}$ = 5.437, p = .025; Bonferroni post hoc comparison, $^{*}p < .05$. **(N)** EPM open arm entries. Same sample size as in panel **(M)**. Two-way ANOVA; main effect of CRS: $F_{1,38}$ = 5.412, p = .025; main effect of vector injection: $F_{1,38}$ = 9.166, p = .004; interaction: $F_{1,38}$ = 4.835, p = .034; Bonferroni post hoc comparison, $^{*}p < .05$, $^{**}p < .01$. **(O)** Representative activity tracking in the open field test (OFT) in mCherry-only and SK2-mCherry mice. **(P)** OFT center time. mCherry-only: n = 10 control mice, n = 10 CRS mice; SK2-mCherry: n = 10 control mice, n = 11 CRS mice. Two-way ANOVA; main effect of CRS: $F_{1,37}$ = 5.753, p = .022; main effect of vector injection: $F_{1,37}$ = 5.132, p = .029; interaction: $F_{1,37}$ = 3.002, p = .092; Bonferroni post hoc comparison, $^{*}p < .05$. **(Q)** OFT total distance traveled. Same sample size as in panel **(P)**. Two-way ANOVA; main effect of CRS: $F_{1,37}$ = 0.295, p = .590; main effect of vector injection: $F_{1,37}$ = 2.457, p = .126; interaction: $F_{1,37}$ = 3.666, p = .063. Pooled data are presented as mean ± SEM. DO, double-floxed orientation; EYFP, enhanced yellow fluorescent protein; IRES, internal ribosome entry site.

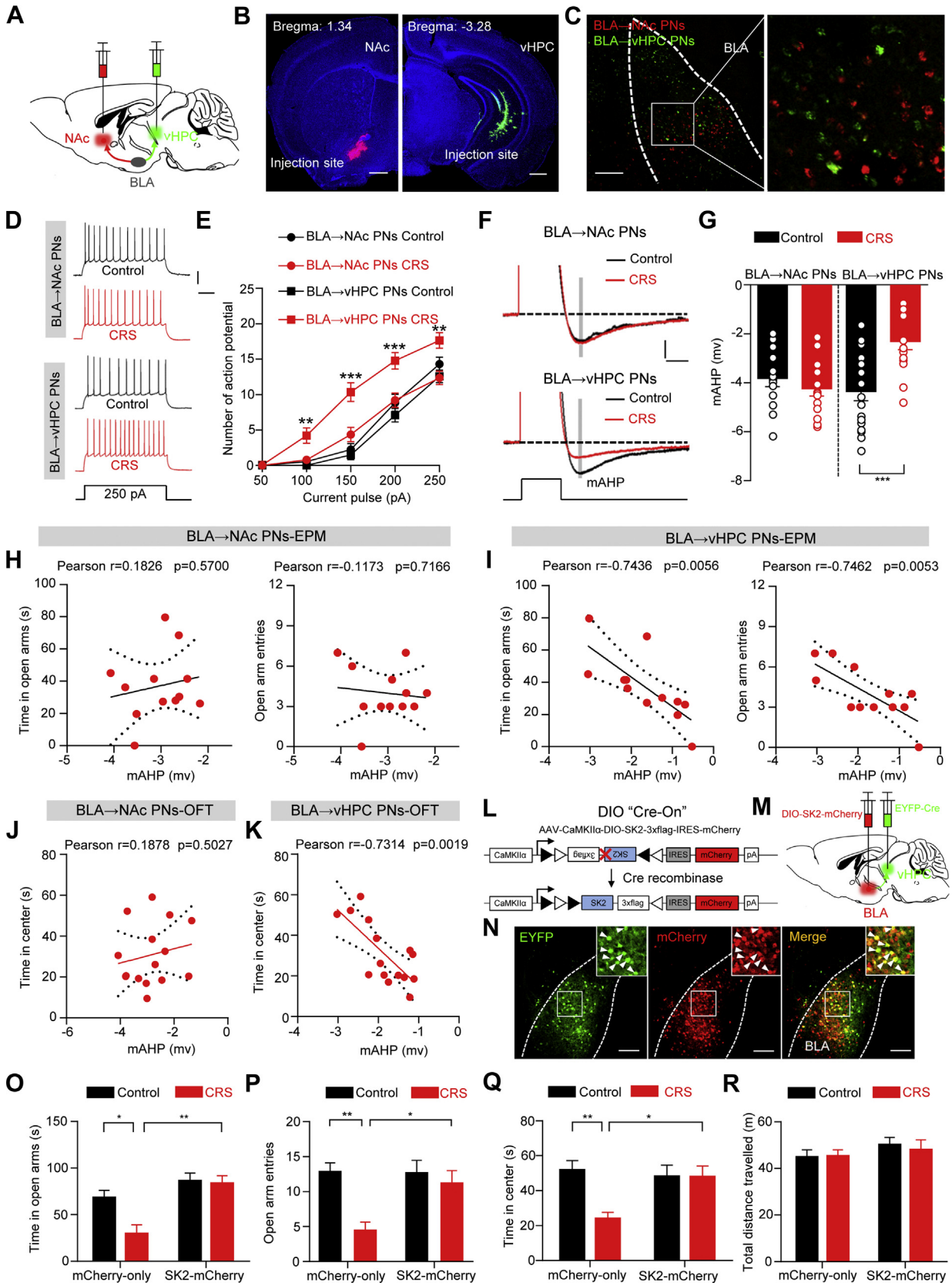
A
NAc
vHPC
BLA
B
Bregma: 1.34
NAc
Injection site
Bregma: -3.28
vHPC
Injection site
C
BLA→NAc PNs
BLA→vHPC PNs
BLA
D
BLA→NAc PNs
Control
CRS
BLA→vHPC PNs
Control
CRS
250 pA
E
BLA→NAc PNs Control
BLA→NAc PNs CRS
BLA→vHPC PNs Control
BLA→vHPC PNs CRS
Number of action potential
Current pulse (pA)
F
BLA→NAc PNs
Control
CRS
BLA→vHPC PNs
Control
CRS
mAHP
G
Control
CRS
BLA→NAc PNs
BLA→vHPC PNs
mAHP (mv)
BLA→NAc PNs-EPM
H
Pearson r=0.1826 p=0.5700
Pearson r=-0.1173 p=0.7166
Time in open arms (s)
Open arm entries
mAHP (mv)
BLA→vHPC PNs-EPM
I
Pearson r=-0.7436 p=0.0056
Pearson r=-0.7462 p=0.0053
Time in open arms (s)
Open arm entries
mAHP (mv)
BLA→NAc PNs-OFT
J
Pearson r=0.1878 p=0.5027
Time in center (s)
mAHP (mv)
BLA→vHPC PNs-OFT
K
Pearson r=-0.7314 p=0.0019
Time in center (s)
mAHP (mv)
L
DIO "Cre-On"
AAV-CaMKIIα-DIO-SK2-3xflag-IRES-mCherry
CaMKIIα
SK2
IRES
mCherry
pA
Cre recombinase
CaMKIIα
SK2
3xflag
IRES
mCherry
pA
M
DIO-SK2-mCherry
EYFP-Cre
vHPC
BLA
N
EYFP
mCherry
Merge
BLA
O
Control
CRS
Time in open arms (s)
mCherry-only
SK2-mCherry
P
Control
CRS
Open arm entries
mCherry-only
SK2-mCherry
Q
Control
CRS
Time in center (s)
mCherry-only
SK2-mCherry
R
Control
CRS
Total distance travelled (m)
mCherry-only
SK2-mCherry

functional integrity of certain input and output pathways to the mPFC would be an attractive mechanism to conserve essential processes that are reliant on these circuits, including the finely tuned, reciprocal BLA-dmPFC network subserving emotional regulation, among other critical functions. On the other hand, the mPFC is generally considered a locus of stress vulnerability (6,11). Based on current and earlier data, it appears that prevailing conceptualizations of the effects of stress on the mPFC need to be refined to accommodate a high degree of circuit specificity and a preservation of the integrity of the BLA→dmPFC circuit under chronic stress.

Another important observation in the current study was the identification of the SK2 channel as a potential mechanism underpinning the circuit-specific effects of stress. As a key regulator of amygdala neuronal activity (51), SK channel has been shown in prior work to be involved in neuronal adaptation to chronic stress in multiple regions (52–54). Specifically, CRS led to SK channel downregulation and a corresponding neuronal hyperexcitability in the lateral amygdala (55), whereas chronic social isolation upregulated SK channels (SK2 and SK3) in dorsal raphe nucleus 5-HT neurons (52). Moreover, BLA-wide viral overexpression of SK2 reduced basal anxiety-like behavior and prevented CRS-induced dendritic hypertrophy and corticosterone secretion (56).

By demonstrating selective SK channel downregulation in BLA→vHPC PNs after CRS and the sufficiency of selective SK expression in this pathway to protect against CRS-related neuronal hyperexcitability and anxiety-like behavior, our data now identify the SK channel, and specifically the SK2 subtype, as a key player driving the heterogeneous effects of CRS on BLA PNs. The identification of the BLA→vHPC pathway as a major locus underlying these effects is in and of itself highly noteworthy, given growing evidence implicating this circuit in stress and anxiety-related behavior (31,40). Whereas glucocorticoids and corticotropin-releasing factor are known regulators of SK channel expression and function (57,58), an important avenue for future studies will be to elucidate the upstream and downstream molecular pathways mediating stress-induced SK channel alterations in this neural circuit.

ACKNOWLEDGMENTS AND DISCLOSURES

This work was supported by the National Natural Science Foundation of China (Grant Nos. 81741759 [to B-XP], 81601179 [to W-HZ], 81503079 [to J-YZ], and 31700916 [to Z-PL]), National Basic Research Program of China (Grant No. 2014CB846100 [to B-XP]), and Natural Science Foundation of Jiangxi Province (Grant Nos. 20172BCB22005 [to B-XP], KJLD14013 [to B-XP], 20161BAB215204 [J-YZ], and 20171BAB214022 [to W-HZ]), and National Institute on Alcohol Abuse and Alcoholism Intramural Research Program (to AH).

W-HZ, W-ZL, YH, W-JY, and J-YZ conducted the experiment. HX and X-LT analyzed the immunohistochemical data. B-ML and LM contributed to the resources. W-HZ, AH, and B-XP designed the experiments and wrote the article.

The authors report no biomedical financial interests or potential conflicts of interest.

ARTICLE INFORMATION

From the Laboratory of Fear and Anxiety Disorders (W-HZ, W-ZL, YH, W-JY, J-YZ, HX, B-ML, B-XP), Institutes of Life Science; Human Aging Research Institute (X-LT), School of Life Science; and Department of Neurology (B-XP), Second Affiliated Hospital, Nanchang University, Nanchang, China; Department of Neurosciences (LM), School of Medicine, Case Western Reserve University; Louis Stokes Cleveland Veterans Affairs Medical Center (LM), Cleveland, Ohio; and Laboratory of Behavioral and Genomic

Figure 8. Stress-induced anxiety-like behavior is associated with small-conductance, calcium-activated potassium (SK) channel downregulation in ventral hippocampus (vHPC)–projecting basolateral amygdala (BLA) projection neurons (PNs). **(A)** Schematic showing injection of red Retrobeads into nucleus accumbens (NAc) and green Retrobeads into vHPC. **(B)** Representative images showing the injection sites in the NAc (left panel) and vHPC (right panel). Scale bar = 500 μm. **(C)** Representative images showing fluorescently-labeled BLA→NAc PNs and BLA→vHPC PNs in BLA. Note that the majority of the two PN populations are spatially segregated. Scale bar = 200 μm. **(D)** Representative traces showing the firing of BLA→NAc PNs and BLA→vHPC PNs to depolarizing current injection. Scale bar = 200 ms, 30 mV. **(E)** Plot of the action potential number in BLA→NAc PNs and BLA→vHPC PNs against the injected current strength. For BLA→NAc PNs, control: n = 13 neurons/4 mice; chronic restraint stress (CRS): n = 14 neurons/5 mice. Two-way analysis of variance (ANOVA) with repeated measures; main effect of CRS: $F_{1,25} = 0.033$, $p = .857$; main effect of current injection: $F_{4,100} = 205.3$, $p < .001$; interaction: $F_{4,100} = 3.264$, $p = .015$. For BLA→vHPC PNs, control: n = 12 neurons/4 mice; CRS: n = 14 neurons/5 mice. Two-way ANOVA with repeated measures; main effect of CRS: $F_{1,24} = 23.820$, $p < .001$; main effect of current injection: $F_{4,96} = 232.3$, $p < .001$; interaction: $F_{4,96} = 17.61$, $p < .001$; Bonferroni post hoc comparison, $^{**}p < .01$; $^{***}p < .001$. **(F)** Representative traces showing medium afterhyperpolarization (mAHP) in BLA→NAc PNs and BLA→vHPC PNs. Scale bar = 100 ms, 2 mV. **(G)** Summary of data shown in panel **(F)**. Data from individual cells are shown as circles, and the mean is shown as a bar. For BLA→NAc PNs, control: n = 15 neurons/4 mice; CRS mice: n = 14 neurons/4 mice. For BLA→vHPC PNs, control: n = 17 neurons/5 mice; CRS mice: n = 15 neurons/5 mice. Two-way ANOVA; main effect of CRS: $F_{1,57} = 5.613$, $p = .021$; main effect of neuron subsets: $F_{1,57} = 4.107$, $p = .047$; interaction: $F_{1,57} = 12.85$, $p < .001$; Bonferroni post hoc comparison, $^{***}p < .001$. **(H)** Correlations between mAHP in BLA→NAc PNs and elevated plus maze (EPM) open arm time and entries in CRS mice. n = 12 mice. **(I)** Correlations between mAHP in BLA→vHPC PNs and EPM open arm time and entries in CRS mice. n = 12 mice. **(J)** Correlations between mAHP in BLA→NAc PNs and open field test (OFT) center time in CRS mice. n = 15 mice. **(K)** Correlations between mAHP in BLA→vHPC PNs and OFT center time in CRS mice. n = 15 mice. Pooled data are presented as mean ± SEM. **(L)** Using Cre-On viral strategy to express SK2 channel in BLA→vHPC PNs. **(M)** Schematic showing injection of rAAV$_2$-retro-*syn*-EYFP-Cre into vHPC and AAV$_{2/8}$-*CaMKIIα*-DIO-SK2-3xFlag-mCherry or AAV$_{2/8}$-*CaMKIIα*-DIO-3xFlag-mCherry into BLA. Injection of rAAV-retro into vHPC results in retrograde transportation of EYFP-Cre to cell bodies of BLA→vHPC PNs, where it drives expression of Cre recombinase inducing SK2 gene expression. **(N)** Representative images showing expression of Cre-recombinase (arrowheads in left panel) and SK2 (arrowheads in middle panel) in BLA neurons. Images are merged in right panel. Scale bar = 100 μmol. **(O)** EPM open arm time in mCherry-only and SK2-mCherry mice. mCherry-only: n = 11 control mice, n = 12 CRS mice; SK2-mCherry: n = 11 control mice, n = 11 CRS mice. Two-way ANOVA; main effect of CRS: $F_{1,41} = 5.660$, $p = .022$; main effect of vector injection: $F_{1,41} = 17.42$, $p < .001$; interaction: $F_{1,42} = 4.312$, $p = .044$; Bonferroni post hoc comparison, $^{*}p < .05$, $^{**}p < .01$. **(P)** EPM open arm entries. Same sample size as in panel **(O)**. Two-way ANOVA; main effect of CRS: $F_{1,41} = 9.999$, $p = .003$; main effect of vector injection: $F_{1,41} = 4.461$, $p = .041$; interaction: $F_{1,41} = 4.967$, $p = .031$; Bonferroni post hoc comparison, $^{*}p < .05$, $^{**}p < .01$. **(Q)** OFT center time in mCherry-only and SK2-mCherry mice. mCherry-only: n = 11 control mice, n = 12 CRS mice; SK2-mCherry: n = 11 control mice, n = 11 CRS mice. Two-way ANOVA; main effect of CRS: $F_{1,41} = 6.536$, $p = .014$; main effect of vector injection: $F_{1,41} = 3.364$, $p = 0.074$; interaction: $F_{1,41} = 6.365$, $p = .016$; Bonferroni post hoc comparison, $^{*}p < .05$, $^{**}p < .01$. **(R)** OFT total distance traveled. Same sample size as in panel **(Q)**. Two-way ANOVA; main effect of CRS: $F_{1,41} = 0.072$, $p = .790$; main effect of vector injection: $F_{1,41} = 1.485$, $p = .230$; interaction: $F_{1,41} = 0.153$, $p = .698$. Pooled data are presented as mean ± SEM. DIO, double-floxed inverted orientation; EYFP, enhanced yellow fluorescent protein; IRES, internal ribosome entry site.

Neuroscience (AH), National Institute on Alcohol Abuse and Alcoholism, National Institutes of Health, Bethesda, Maryland.

Address correspondence to Bing-Xing Pan, Ph.D., M.D., Laboratory of Fear and Anxiety Disorders, Institutes of Life Science, Nanchang University, Nanchang, 330031, China; E-mail: panbingxing@ncu.edu.cn.

Received Aug 23, 2018; revised Nov 17, 2018; accepted Dec 5, 2018.

Supplementary material cited in this article is available online at https://doi.org/10.1016/j.biopsych.2018.12.010.

REFERENCES

1. Hermans EJ, Henckens MJ, Joels M, Fernandez G (2014): Dynamic adaptation of large-scale brain networks in response to acute stressors. Trends Neurosci 37:304–314.
2. Young CB, Raz G, Everaerd D, Beckmann CF, Tendolkar I, Hendler T, *et al.* (2017): Dynamic shifts in large-scale brain network balance as a function of arousal. J Neurosci 37:281–290.
3. van Marle HJ, Hermans EJ, Qin S, Fernandez G (2009): From specificity to sensitivity: How acute stress affects amygdala processing of biologically salient stimuli. Biol Psychiatry 66:649–655.
4. Roozendaal B, McEwen BS, Chattarji S (2009): Stress, memory and the amygdala. Nat Rev Neurosci 10:423–433.
5. Maier SU, Makwana AB, Hare TA (2015): Acute stress impairs self-control in goal-directed choice by altering multiple functional connections within the brain's decision circuits. Neuron 87:621–631.
6. Arnsten AF (2009): Stress signalling pathways that impair prefrontal cortex structure and function. Nat Rev Neurosci 10:410–422.
7. Qin S, Hermans EJ, van Marle HJ, Luo J, Fernandez G (2009): Acute psychological stress reduces working memory-related activity in the dorsolateral prefrontal cortex. Biol Psychiatry 66:25–32.
8. Henckens MJ, van Wingen GA, Joels M, Fernandez G (2010): Time-dependent effects of corticosteroids on human amygdala processing. J Neurosci 30:12725–12732.
9. Yuen EY, Liu W, Karatsoreos IN, Feng J, McEwen BS, Yan Z (2009): Acute stress enhances glutamatergic transmission in prefrontal cortex and facilitates working memory. Proc Natl Acad Sci U S A 106: 14075–14079.
10. Liu ZP, Song C, Wang M, He Y, Xu XB, Pan HQ, *et al.* (2014): Chronic stress impairs GABAergic control of amygdala through suppressing the tonic GABAA receptor currents. Mol Brain 7:32.
11. Chattarji S, Tomar A, Suvrathan A, Ghosh S, Rahman MM (2015): Neighborhood matters: Divergent patterns of stress-induced plasticity across the brain. Nat Neurosci 18:1364–1375.
12. Dias-Ferreira E, Sousa JC, Melo I, Morgado P, Mesquita AR, Cerqueira JJ, *et al.* (2009): Chronic stress causes frontostriatal reorganization and affects decision-making. Science 325:621–625.
13. Gold PW (2015): The organization of the stress system and its dysregulation in depressive illness. Mol Psychiatry 20:32–47.
14. Craske MG, Stein MB, Eley TC, Milad MR, Holmes A, Rapee RM, *et al.* (2017): Anxiety disorders. Nat Rev Dis Primers 3:17024.
15. Ramirez S, Tonegawa S, Liu X (2013): Identification and optogenetic manipulation of memory engrams in the hippocampus. Front Behav Neurosci 7:226.
16. Beyeler A, Namburi P, Glober GF, Simonnet C, Calhoon GG, Conyers GF, *et al.* (2016): Divergent routing of positive and negative information from the amygdala during memory retrieval. Neuron 90:348–361.
17. Xu C, Krabbe S, Grundemann J, Botta P, Fadok JP, Osakada F, *et al.* (2016): Distinct hippocampal pathways mediate dissociable roles of context in memory retrieval. Cell 167:961–972.e916.
18. Grewe BF, Grundemann J, Kitch LJ, Lecoq JA, Parker JG, Marshall JD, *et al.* (2017): Neural ensemble dynamics underlying a long-term associative memory. Nature 543:670–675.
19. Lowery-Gionta EG, Crowley NA, Bukalo O, Silverstein S, Holmes A, Kash TL (2018): Chronic stress dysregulates amygalar output to the prefrontal cortex. Neuropharmacology 139:68–75.
20. Namburi P, Beyeler A, Yorozu S, Calhoon GG, Halbert SA, Wichmann R, *et al.* (2015): A circuit mechanism for differentiating positive and negative associations. Nature 520:675–678.
21. Stuber GD, Sparta DR, Stamatakis AM, van Leeuwen WA, Hardjoprajitno JE, Cho S, *et al.* (2011): Excitatory transmission from the amygdala to nucleus accumbens facilitates reward seeking. Nature 475:377–380.
22. Burgos-Robles A, Kimchi EY, Izadmehr EM, Porzenheim MJ, Ramos-Guasp WA, Nieh EH, *et al.* (2017): Amygdala inputs to prefrontal cortex guide behavior amid conflicting cues of reward and punishment. Nat Neurosci 20:824–835.
23. Gold AL, Morey RA, McCarthy G (2015): Amygdala-prefrontal cortex functional connectivity during threat-induced anxiety and goal distraction. Biol Psychiatry 77:394–403.
24. Mitra R, Jadhav S, McEwen BS, Vyas A, Chattarji S (2005): Stress duration modulates the spatiotemporal patterns of spine formation in the basolateral amygdala. Proc Natl Acad Sci U S A 102:9371–9376.
25. Maroun M, Ioannides PJ, Bergman KL, Kavushansky A, Holmes A, Wellman CL (2013): Fear extinction deficits following acute stress associates with increased spine density and dendritic retraction in basolateral amygdala neurons. Eur J Neurosci 38:2611–2620.
26. Zhang JY, Liu TH, He Y, Pan HQ, Zhang WH, Yin XP, *et al.* (2019): Chronic stress remodels synapses in an amygdala circuit-specific manner. Biol Psychiatry 85:189–201.
27. Cho JH, Deisseroth K, Bolshakov VY (2013): Synaptic encoding of fear extinction in mPFC-amygdala circuits. Neuron 80:1491–1507.
28. Linden DE (2006): How psychotherapy changes the brain—the contribution of functional neuroimaging. Mol Psychiatry 11:528–538.
29. Mpari B, Regaya I, Escoffier G, Mourre C (2005): Differential effects of two blockers of small conductance Ca2+-activated K+ channels, apamin and lei-Dab7, on learning and memory in rats. J Integr Neurosci 4:381–396.
30. Tacconi S, Carletti R, Bunnemann B, Plumpton C, Merlo Pich E, Terstappen GC (2001): Distribution of the messenger RNA for the small conductance calcium-activated potassium channel SK3 in the adult rat brain and correlation with immunoreactivity. Neuroscience 102:209–215.
31. Felix-Ortiz AC, Beyeler A, Seo C, Leppla CA, Wildes CP, Tye KM (2013): BLA to vHPC inputs modulate anxiety-related behaviors. Neuron 79:658–664.
32. Melia KR, Ryabinin AE, Schroeder R, Bloom FE, Wilson MC (1994): Induction and habituation of immediate early gene expression in rat brain by acute and repeated restraint stress. J Neurosci 14:5929–5938.
33. Song C, Zhang WH, Wang XH, Zhang JY, Tian XL, Yin XP, *et al.* (2017): Acute stress enhances the glutamatergic transmission onto basoamygdala neurons embedded in distinct microcircuits. Mol Brain 10:3.
34. McGarry LM, Carter AG (2016): Inhibitory gating of basolateral amygdala inputs to the prefrontal cortex. J Neurosci 36:9391–9406.
35. Marek R, Jin J, Goode TD, Giustino TF, Wang Q, Acca GM, *et al.* (2018): Hippocampus-driven feed-forward inhibition of the prefrontal cortex mediates relapse of extinguished fear. Nat Neurosci 21: 384–392.
36. Garcia R, Vouimba RM, Baudry M, Thompson RF (1999): The amygdala modulates prefrontal cortex activity relative to conditioned fear. Nature 402:294–296.
37. Vyas A, Mitra R, Shankaranarayana Rao BS, Chattarji S (2002): Chronic stress induces contrasting patterns of dendritic remodeling in hippocampal and amygdaloid neurons. J Neurosci 22:6810–6818.
38. Hoffman AN, Parga A, Paode PR, Watterson LR, Nikulina EM, Hammer RP Jr, *et al.* (2015): Chronic stress enhanced fear memories are associated with increased amygdala zif268 mRNA expression and are resistant to reconsolidation. Neurobiol Learn Mem 120:61–68.
39. Suvrathan A, Bennur S, Ghosh S, Tomar A, Anilkumar S, Chattarji S (2014): Stress enhances fear by forming new synapses with greater capacity for long-term potentiation in the amygdala. Philos Trans R Soc Lond B Biol Sci 369:20130151.
40. Ghosh S, Laxmi TR, Chattarji S (2013): Functional connectivity from the amygdala to the hippocampus grows stronger after stress. J Neurosci 33:7234–7244.
41. Hariri AR, Holmes A (2015): Finding translation in stress research. Nat Neurosci 18:1347–1352.

42. Han JH, Kushner SA, Yiu AP, Cole CJ, Matynia A, Brown RA, *et al.* (2007): Neuronal competition and selection during memory formation. Science 316:457–460.
43. Kim J, Pignatelli M, Xu S, Itohara S, Tonegawa S (2016): Antagonistic negative and positive neurons of the basolateral amygdala. Nat Neurosci 19:1636–1646.
44. Fadok JP, Krabbe S, Markovic M, Courtin J, Xu C, Massi L, *et al.* (2017): A competitive inhibitory circuit for selection of active and passive fear responses. Nature 542:96–100.
45. Beyeler A, Chang CJ, Silvestre M, Leveque C, Namburi P, Wildes CP, *et al.* (2018): Organization of valence-encoding and projection-defined neurons in the basolateral amygdala. Cell Rep 22:905–918.
46. Senn V, Wolff SB, Herry C, Grenier F, Ehrlich I, Grundemann J, *et al.* (2014): Long-range connectivity defines behavioral specificity of amygdala neurons. Neuron 81:428–437.
47. Felix-Ortiz AC, Burgos-Robles A, Bhagat ND, Leppla CA, Tye KM (2016): Bidirectional modulation of anxiety-related and social behaviors by amygdala projections to the medial prefrontal cortex. Neuroscience 321:197–209.
48. Sotres-Bayon F, Sierra-Mercado D, Pardilla-Delgado E, Quirk GJ (2012): Gating of fear in prelimbic cortex by hippocampal and amygdala inputs. Neuron 76:804–812.
49. Shansky RM, Hamo C, Hof PR, McEwen BS, Morrison JH (2009): Stress-induced dendritic remodeling in the prefrontal cortex is circuit specific. Cereb Cortex 19:2479–2484.
50. Chaudhury D, Walsh JJ, Friedman AK, Juarez B, Ku SM, Koo JW, *et al.* (2013): Rapid regulation of depression-related behaviours by control of midbrain dopamine neurons. Nature 493:532–536.
51. Faber ES, Delaney AJ, Sah P (2005): SK channels regulate excitatory synaptic transmission and plasticity in the lateral amygdala. Nat Neurosci 8:635–641.
52. Sargin D, Oliver DK, Lambe EK (2016): Chronic social isolation reduces 5-HT neuronal activity via upregulated SK3 calcium-activated potassium channels. Elife 5.
53. Rau AR, Chappell AM, Butler TR, Ariwodola OJ, Weiner JL (2015): Increased basolateral amygdala pyramidal cell excitability may contribute to the anxiogenic phenotype induced by chronic early-life stress. J Neurosci 35:9730–9740.
54. Atchley D, Hankosky ER, Gasparotto K, Rosenkranz JA (2012): Pharmacological enhancement of calcium-activated potassium channel function reduces the effects of repeated stress on fear memory. Behav Brain Res 232:37–43.
55. Rosenkranz JA, Venheim ER, Padival M (2010): Chronic stress causes amygdala hyperexcitability in rodents. Biol Psychiatry 67: 1128–1136.
56. Mitra R, Ferguson D, Sapolsky RM (2009): SK2 potassium channel overexpression in basolateral amygdala reduces anxiety, stress-induced corticosterone secretion and dendritic arborization. Mol Psychiatry 14:847–855, 827.
57. Kye MJ, Spiess J, Blank T (2007): Transcriptional regulation of intronic calcium-activated potassium channel SK2 promoters by nuclear factor-kappa B and glucocorticoids. Mol Cell Biochem 300:9–17.
58. Authement ME, Langlois LD, Shepard RD, Browne CA, Lucki I, Kassis H, *et al.* (2018): A role for corticotropin-releasing factor signaling in the lateral habenula and its modulation by early-life stress. Sci Signal 11.